Networks and Heterogeneous Media

http://www.aimspress.com/journal/nhm

NHM, 19(1): 44–85.
DOI: 10.3934/nhm.2024003
Received: 12 November 2023
Revised: 27 December 2023
Accepted: 08 January 2024
Published: 12 January 2024

Research article

Application of a hybrid pseudospectral method to a new two-dimensional multi-term mixed sub-diffusion and wave-diffusion equation of fractional order

Farman Ali Shah[1], Kamran[1,*], Dania Santina[2], Nabil Mlaiki[2] and Salma Aljawi[3]

[1] Department of Mathematics, Islamia College Peshawar, Jamrod Road, Peshawar 25120, Khyber PakhtunKhwa, Pakistan
[2] Department of Mathematics and Sciences, Prince Sultan University, Riyadh 11586, Saudi Arabia
[3] Department of Mathematical Sciences, Princess Nourah Bint Abdulrahman University, Riyadh, PO Box 84428, Saudi Arabia

* **Correspondence:** Email: dsantina@psu.edu.sa, nmlaiki@psu.edu.sa.

Abstract: In the current study, a novel multi-term mixed sub-diffusion and wave-diffusion model was considered. The new model has a unique time-space coupled derivative in addition to having the diffusion-wave and sub-diffusion terms concurrently. Typically, an elliptic equation in the space variable is obtained by applying a finite difference time-stepping procedure. The severe stability restrictions are the main disadvantage of the finite difference method in time. It has been demonstrated that the Laplace transform is an excellent choice for solving diffusion problems and offers a substitute to the finite difference approach. In this paper, a method based on Laplace transform coupled with the pseudospectral method was developed for the novel model. The proposed method has three main steps: First, the model was reduced to a time-independent model via Laplace transform; second, the pseudospectral method was employed for spatial discretization; and finally, the inverse Laplace transform was applied to transform the obtained solution in Laplace transform domain back into a real domain. We also presented the numerical scheme's stability and convergence analysis. To demonstrate our method's efficacy, four problems were examined.

Keywords: mixed sub-diffusion and diffusion-wave equation; Caputo's derivative; Laplace transform; pseudospectral method; Talbot's method

1. Introduction

Time-fractional partial differential equations (TFPDEs) have attracted considerable attention due to their ability to model memory and nonlocal properties. It has been established that TFPDEs are crucial mathematical and physical models for describing a wide range of anomalous phenomena and complex systems in the fields of natural science and engineering [1–5]. Successful applications of TFPDEs include signal processing [6], Powell-Eyring fluid [7], fluid mechanics [8, 9], and robotics [10]. The multi-term TFPDEs have been found useful in describing many complex natural phenomena, such as magnetic resonance imaging (MRI) [11], viscoelastic mechanical models [12], and oxygen delivery through capillaries to a tissue (see [13] and the references therein). The multi-term time-fractional mixed sub-diffusion and diffusion wave equations belong to an important class of multi-term TFPDEs that have three major subclasses: the time-fractional sub-diffusion equations (TFSDEs), whose fractional order belongs to $(0, 1)$; the time fractional diffusion-wave equations (TFDWEs), whose fractional order belongs to $(1, 2)$; and TFDEs whose fractional order belongs to $(0, 2)$. Some researchers studied the analytical solutions of these equations, such as the authors of [14] who studied the solution of multi-term TFDWEs using the method of separation of variables. In [15], the authors used the Laguerre polynomials for obtaining the approximate solution of 1D TFDWE. The authors of [16] obtained the analytic solution of the multi-term space-time fractional advection-diffusion equation using a method based on spectral representation of fractional Laplacian operator. In most cases, the analytical solution of the these equations is provided in terms of special functions such as the multivariate Mittag-Leffler function and the Fox H-function [17, 18], which are very complex and challenging to evaluate. Therefore, to solve these equations, numerical methods would be preferable, particularly in situations where analytical solutions are not present. Various numerical schemes have been developed to solve TFPDEs. Liu et al. [19] developed a first-order finite difference approach with stability constraints for both time and spatial derivatives. The multi-term time-fractional mixed sub-diffusion with a variable coefficient was introduced by Zhao [20] using the finite element method. The solution of the wave-diffusion equation based on the Legendre spectral method and finite difference method for discretization of space and time derivatives was established in [21]. Shen and Gu [22] developed two novel finite difference schemes for 2D time fractional mixed diffusion and wave-diffusion equations. Agrawal [23] utilized the Laplace transform and finite sine transform for obtaining the solution of the wave-diffusion equation. In [24], the authors coupled spatial extrapolation method with the Crank-Nicholson method to obtain the solution to the fractional diffusion problem. In [25], a fully discrete spectral method was employed for the solution of a novel multi-term time-fractional mixed diffusion and diffusion-wave equation. The mesh-less method based on radial basis function was employed by [26] for the approximate solution of multi-term time-fractional mixed sub-diffusion. In [27], the authors coupled the dual reciprocity method and the improved singular boundary method for multi-term fractional wave-diffusion equations. Ye et al. [28] solved the 2D and 3D multi-term time-space fractional diffusion equations via a series expansion. Li et al. [29] analyzed the temporal asymptotic behavior with well-posedness for the solution of the multi-term time-fractional diffusion equation. The authors of [30] employed the spectral method for the numerical solution of the two-dimensional multi-term time-fractional mixed sub-diffusion. Sun [31] examined the simultaneous inversion of the potential term and the fractional orders in a multi-term time-fractional diffusion equation. Spectral methods are among the most popular techniques for discretizing spatial variables in partial differential equations, which have the reputation of producing extremely accurate approximations of sufficiently smooth solutions [32, 33]. Over time, spectral methods have been widely used in many fields, such as quantum mechanics [34], fluid dynamics [35], weather forecasting [36], and heat conduction [37], due to their high-order accuracy. These techniques haven't, however, been applied to many problems where the finite-difference and finite-element approaches are still frequently used because of some disadvantages. One disadvantage is that using spectral methods to discretize partial differential equations results in the solution of large systems of linear or nonlinear equations that require full matrices. On the other hand, finite-difference and finite-element approaches produce sparse matrices, which can be handled by suitable techniques to significantly reduce the computational complexity. Another drawback of spectral methods is that they face difficulties for problems defined on complex geometries. Although, some authors have attempted to use spectral methods in complex geometries [38, 39]. In this work, our aim is to obtain the approximate solution of the multi-term time-fractional mixed sub-diffusion using the pseudospectral method in space coupled with the Laplace transform in time. The pseudospectral method is an easy method to implement and offers low computational cost with high accuracy. Also, it has been proven that for time discretization, the Laplace transform is suitable for solving various initial and boundary value problems and can be utilized as an alternative to the classical time stepping techniques [40]. In finite difference time stepping techniques, the accuracy can be obtained for extremely short time steps, which results in high computational cost and crucial stability constraints. A large number of valuable works are available in the literature, which couples Laplace transform in time with another method in space (see [41, 42] and references therein). In this article, we consider a two-dimensional multi-term time-fractional mixed sub-diffusion and diffusion-wave equation of the following form [43]:

$$\begin{aligned}\sum_{k=1}^{p}\varrho_{1,k}\frac{\partial^{\alpha_k}u(\bar{\boldsymbol{\xi}},t)}{\partial t^{\alpha_k}}+\varrho_2 D_t u(\bar{\boldsymbol{\xi}},t)+\sum_{r=1}^{q}\varrho_{3,r}\frac{\partial^{\beta_r}u(\bar{\boldsymbol{\xi}},t)}{\partial t^{\beta_r}}+\varrho_4 u(\bar{\boldsymbol{\xi}},t)&=\varrho_5\Delta u(\bar{\boldsymbol{\xi}},t)\\ &+\varrho_6\frac{\partial^{\gamma}\Delta u(\bar{\boldsymbol{\xi}},t)}{\partial t^{\gamma}}+\mathcal{G}(\bar{\boldsymbol{\xi}},t),\ \bar{\boldsymbol{\xi}}\in\Gamma,\ t\in[0,1]\end{aligned} \tag{1.1}$$

with boundary conditions

$$\mathcal{L}_{\mathcal{B}}u(\bar{\boldsymbol{\xi}},t)=h(\bar{\boldsymbol{\xi}},t),\ \bar{\boldsymbol{\xi}}\in\partial\Gamma,\ t\in[0,1] \tag{1.2}$$

and initial condition

$$u(\bar{\boldsymbol{\xi}},0)=g_1(\bar{\boldsymbol{\xi}}),u_t(\bar{\boldsymbol{\xi}},0)=g_2(\bar{\boldsymbol{\xi}}),\ \bar{\boldsymbol{\xi}}\in\Gamma \tag{1.3}$$

where $\mathcal{G}(\bar{\boldsymbol{\xi}},t),\ g_1(\bar{\boldsymbol{\xi}}),\ g_2(\bar{\boldsymbol{\xi}}),\ h(\bar{\boldsymbol{\xi}},t)$ are given continuous functions, $\varrho_{1,k}>0, \varrho_{3,r}>0,\ \varrho_l>0,\ l=2,4,5,6$, the coefficients are not simultaneously equal to zero, $1<\alpha_1<\alpha_2<...<\alpha_p<2,\ 0<\beta_1<\beta_2<...<\beta_q<1,\ 0<\gamma<1, \bar{\boldsymbol{\xi}}=(\xi,\zeta),\ D_t=\frac{\partial}{\partial t},\ \Delta=\frac{\partial^2}{\partial\xi^2}+\frac{\partial^2}{\partial\zeta^2},\ \mathcal{L}_{\mathcal{B}}$ is the boundary operator, $\Gamma\subset\mathbb{R}^2$ is the domain, $\partial\Gamma$ is its boundary, and $\frac{\partial^{\alpha}u(\bar{\boldsymbol{\xi}},t)}{\partial t^{\alpha}}$, $\frac{\partial^{\beta}u(\bar{\boldsymbol{\xi}},t)}{\partial t^{\beta}}$, and $\frac{\partial^{\gamma}u(\bar{\boldsymbol{\xi}},t)}{\partial t^{\gamma}}$ are fractional derivatives in Caputo's sense, defined as in [44].

$$\frac{\partial^{\alpha}u(\bar{\boldsymbol{\xi}},t)}{\partial t^{\alpha}}=\frac{1}{\Gamma(n-\alpha)}\int_0^t\frac{\frac{\partial^n u(\bar{\boldsymbol{\xi}},\nu)}{\partial\nu^n}}{(t-\nu)^{\alpha-n+1}}d\nu,\ n-1<\alpha\le n$$

In literature, there are many physical processes whose characteristics cannot be described by utilizing the time fractional sub-diffusion equations or the time fractional wave diffusion equation independently. In order to avoid such limitations, the multi-term time-fractional mixed sub-diffusion can be utilized as an effective mathematical model [43]. These models are particularly beneficial at representing anomalous diffusion processes and capturing the properties of media, including power-law frequency dependence [30]. Additionally, they are proficient in the modeling of various types of viscoelastic damping, modeling the unsteady flow of a fractional Maxwell fluid [45], and describing the behavior of an Oldroyd-B fluid, which has been used to simulate the response of many dilute polymeric liquids [22].

1.1. Laplace transform

In this section, the Laplace transform is employed on the multi-term time fractional mixed sub-diffusion and diffusion-wave equation in order to reduce the problem into an equivalent time-independent problem. The Laplace transform of $u(\bar{\boldsymbol{\xi}}, t)$ is denoted and defined as in [44]

$$\widehat{u}(\bar{\boldsymbol{\xi}}, s) = \int_0^\infty e^{-st} u(\bar{\boldsymbol{\xi}}, t) dt$$

The Laplace transform of Caputo's derivative $\frac{\partial^\alpha u(\bar{\boldsymbol{\xi}},t)}{\partial t^\alpha}$ of fractional order $\alpha \in (m-1, m]$ is defined as in [44]

$$L\left\{\frac{\partial^\alpha u(\bar{\boldsymbol{\xi}}, t)}{\partial t^\alpha}\right\} = s^\alpha \widehat{u}(\bar{\boldsymbol{\xi}}, s) - \sum_{j=0}^{m-1} s^{\alpha-j-1} u^{(j)}(\bar{\boldsymbol{\xi}}, 0)$$

Applying Laplace transform on Eqs (1.1)–(1.3), we have

$$\begin{aligned}\sum_{k=1}^{p} \varrho_{1,k}\Big(s^{\alpha_k}\widehat{u}(\bar{\boldsymbol{\xi}}, s) - s^{\alpha_k-1}u(\bar{\boldsymbol{\xi}}, 0) - s^{\alpha_k-2}u_t(\bar{\boldsymbol{\xi}}, 0)\Big) + \varrho_2(s\widehat{u}(\bar{\boldsymbol{\xi}}, s)\\ -u(\bar{\boldsymbol{\xi}}, 0)) + \sum_{r=1}^{q} \varrho_{3,r}\Big(s^{\beta_r}\widehat{u}(\bar{\boldsymbol{\xi}}, s) - s^{\beta_r-1}u(\bar{\boldsymbol{\xi}}, 0)\Big) + \varrho_4\widehat{u}(\bar{\boldsymbol{\xi}}, s)\\ = \varrho_5\mathcal{L}\widehat{u}(\bar{\boldsymbol{\xi}}, s) + \varrho_6(s^\gamma\mathcal{L}\widehat{u}(\bar{\boldsymbol{\xi}}, s) - s^{\gamma-1}\mathcal{L}u(\bar{\boldsymbol{\xi}}, 0)) + \widehat{\mathcal{G}}(\bar{\boldsymbol{\xi}}, s)\end{aligned}$$

and

$$\mathcal{L}_{\mathcal{B}}\widehat{u}(\bar{\boldsymbol{\xi}}, s) = \widehat{h}(\bar{\boldsymbol{\xi}}, s)$$

which implies

$$\left(\sum_{k=1}^{p} \varrho_{1,k}s^{\alpha_k}I + \varrho_2 sI + \sum_{r=1}^{q}\varrho_{3,r}s^{\beta_r}I + \varrho_4 I - \varrho_5\mathcal{L} - \varrho_6 s^\gamma\mathcal{L}\right)\widehat{u}(\bar{\boldsymbol{\xi}}, s) = \widehat{\mathcal{H}}(\bar{\boldsymbol{\xi}}, s) \tag{1.4}$$

$$\mathcal{L}_{\mathcal{B}}\widehat{u}(\bar{\boldsymbol{\xi}}, s) = \widehat{h}(\bar{\boldsymbol{\xi}}, s) \tag{1.5}$$

where $\widehat{\mathcal{H}}(\bar{\boldsymbol{\xi}}, s) = \sum_{k=1}^{p}\varrho_{1,k}s^{\alpha_k-1}g_1(\bar{\boldsymbol{\xi}}) + \sum_{k=1}^{p}\varrho_{1,k}s^{\alpha_k-2}g_2(\bar{\boldsymbol{\xi}}) + \varrho_2 g_1(\bar{\boldsymbol{\xi}}) + \sum_{r=1}^{q}\varrho_{3,r}s^{\beta_r-1}g_1(\bar{\boldsymbol{\xi}})$ $- \varrho_6 s^{\gamma-1}\mathcal{L}g_1(\bar{\boldsymbol{\xi}}) + \widehat{\mathcal{G}}(\bar{\boldsymbol{\xi}}, s)$, $\mathcal{L} = \Delta$, and I is the identity operator. In the proposed approach, first we discretize the linear differential operator $\mathcal{L}$ via the pseudospectral method, then the full-discrete system (Eqs (1.4) and (1.5)) is solved in Laplace transform space. Finally the solution of Eqs (1.1)–(1.3) is obtained via inversion of the Laplace transform. Our solution method is highly suitable for parallel computations; it belongs to the class of parallel in time methods for TFPDEs (see [46]). The pseudospectral method is discussed in next section.

1.2. *Pseudospectral method*

The pseudospectral method is an accurate and extremely precise approach for the numerical solution of TFPDEs. The pseudospectral method uses the Chebyshev points for collocation that are nonzero over the entire domain, whereas finite element methods use basis functions that are nonzero only on small subintervals [35]. In the pseudospectral method, the expansion of solutions is characterized by some global basis functions, such as Lagrange's interpolation polynomials. The concept of interpolation and differentiation matrices [47] is very important in the pseudospectral method. To provide a comprehensive description of the pseudospectral method based on Lagrange's interpolation polynomial basis, the main aspects of the differentiation matrices are reviewed in the next section.

1.2.1. Differentiation matrices

In the pseudospectral method, the solution is considered over $[-1, 1]$ and the data $\left\{\left(\xi_j, \widehat{u}(\xi_j)\right)\right\}_{j=0}^{m}$ is interpolated by the Lagrange polynomial (LP) $\eta_j(\xi)$ of degree $\leq m$ [33, 48]

$$\mathcal{I}_m(\xi) = \sum_{j=0}^{m} \eta_j(\xi)\widehat{u}_j$$

where $\eta_j(\xi)$ is the LP at the point $\xi_j (j = 0, 1, ..., m)$, which is

$$\eta_j(\xi) = \frac{(\xi - \xi_0)...(\xi - \xi_{j-1})(\xi - \xi_{j+1})...(\xi - \xi_m)}{(\xi_j - \xi_0)...(\xi_j - \xi_{j-1})(\xi_j - \xi_{j+1})...(\xi_j - \xi_m)} \tag{1.6}$$

where $\widehat{u}_j = \widehat{u}(\xi_j)$. The Chebyshev nodes are defined as

$$\xi_j = \cos\left(\frac{j\pi}{m}\right), \quad j = 0, 1, ..., m \tag{1.7}$$

and are used to discretize the domain $[-1, 1]$. The 1^{st} derivative $\frac{\partial \widehat{u}(\xi)}{\partial \xi}$ is approximated as

$$\frac{\partial \widehat{u}(\xi)}{\partial \xi} \approx \mathbf{\Phi}_m \widehat{u}$$

and the matrix $\mathbf{\Phi}_m$ has elements in the following form

$$[\mathbf{\Phi}_m]_{i,j} = \eta'_j(\xi_i), \; i, j = 1, 2, ..., m$$

The non-diagonal elements of $[\mathbf{\Phi}_m]_{i,j}$ have the following form

$$[\mathbf{\Phi}_m]_{i,j} = \frac{\alpha_j}{\alpha_i(\xi_i - \xi_j)}, \; i \neq j$$

where $\alpha_j^{-1} = \prod_{i\neq j}^{m}(\xi_i - \xi_j)$, and the elements on diagonal entries are expressed as

$$[\mathbf{\Phi}_m]_{i,j} = - \sum_{j=0, \; j\neq i}^{m} [\mathbf{\Phi}_m]_{i,j}, \; i = 0, 1, 2, .., m$$

The elements of the μth-order derivative of $\mathbf{\Phi}_m^\mu$ are analytically obtained as

$$[\mathbf{\Phi}_m^\mu]_{i,j} = \eta_j^\mu(\xi_i),\ i, j = 1, 2, ..., m$$

In [47,49], more accurate evaluation of the differentiation matrices is elaborated. For the differentiation matrices, Welfert [47] deduced a handy recursion relation as follows

$$[\mathbf{\Phi}_m^\mu]_{kj} = \frac{\mu}{\xi_k - \xi_j}\left(\frac{\alpha_j}{\alpha_k}[\mathbf{\Phi}_m^{(\mu-1)}]_{kk} - [\mathbf{\Phi}_m^{(\mu-1)}]_{kj}\right),\ k \neq j$$

Chebyshev points are remarkable for their ability to enable spectral convergence when appropriate analytic assumptions are made.

1.2.2. The discrete spectral operator

Let us consider the square domain $\Gamma = [-1, 1]^2$. Generally, the point in Γ is denoted by $\bar{\boldsymbol{\xi}}$ and is expressed as

$$\bar{\boldsymbol{\xi}}_{ij} = \left(\cos\left(\frac{\pi i}{m}\right), \cos\left(\frac{\pi j}{m}\right)\right),\ i, j = 0, 1, 2, ..., m$$

The LPs associated to $\bar{\boldsymbol{\xi}}_{ij}$ can be written as

$$\eta_{ij}(\bar{\boldsymbol{\xi}}) = \eta_i(\xi)\eta_j(\zeta)$$

where $\eta_{ij}(\bar{\boldsymbol{\xi}}_{ij}) = \delta_{ij}$. The 2^{nd}-order derivatives of the LPs Eq (1.6) are given as

$$\frac{\partial^2\eta_{ij}(\bar{\boldsymbol{\xi}}_{rs})}{\partial\xi^2} = \eta_i''(\xi_r)\eta_j(\zeta_s) = [\mathbf{\Phi}_m^2]_{ri}\delta_{js},$$
$$\frac{\partial^2\eta_{ij}(\bar{\boldsymbol{\xi}}_{rs})}{\partial\zeta^2} = \eta_i(\xi_r)\eta_j''(\zeta_s) = \delta_{ri}[\mathbf{\Phi}_m^2]_{sj}$$

where $\mathbf{\Phi}_m^2$ represents the second order differentiation matrix based on Chebyshev points. Applying the operator $\mathcal{L}$ on the LPs Eq (1.6) based on the points $\{\bar{\boldsymbol{\xi}}_{rs}\}$ is

$$\mathcal{L}(\eta_{ij}(\bar{\boldsymbol{\xi}}_{rs})) = \left([\mathbf{\Phi}_m^2]_{ri}\delta_{js} + \delta_{ri}[\mathbf{\Phi}_m^2]_{sj}\right)$$

Consequently, the approximation $\mathcal{L}$ via the pseudospectral method is obtained as

$$\mathcal{L}_{\boldsymbol{M}} = \left(I_m \otimes \mathbf{\Phi}_m^2 + \mathbf{\Phi}_m^2 \otimes I_m\right)$$

The conditions in Eq (1.5) are incorporating by considering the interpolation matrix $\mathcal{L}_{\boldsymbol{M}}$ and considering all points $\bar{\boldsymbol{\xi}}$. Furthermore, the rows of $\mathcal{L}_{\boldsymbol{M}}$ in correspondence with boundary nodes are replaced with unit vectors that have a one in accordance with the diagonal elements of $\mathcal{L}_{\boldsymbol{M}}$. Hence, the boundary conditions $\mathcal{L}_{\mathcal{B}}\widehat{u}(\bar{\boldsymbol{\xi}}, s) = \widehat{h}(\bar{\boldsymbol{\xi}}, s)$ in Eq (1.5) will be implemented directly [33]. By rearranging the columns and rows of the matrix $\mathcal{L}_{\boldsymbol{M}}$, the following block matrix is obtained

$$\mathcal{L}_{\partial\Gamma} = \begin{bmatrix} W & R \\ 0 & I \end{bmatrix}$$

where W and I are the nonzero square blocks of order $(m-m_{\mathcal{B}})\times(m-m_{\mathcal{B}})$ and $(m_{\mathcal{B}}\times m_{\mathcal{B}})$, respectively. However, $m_{\mathcal{B}}$ represents the boundary points. The solution of the system Eqs (1.4) and (1.5) can be attained by solving the linear block system

$$\mathcal{L}_{\partial\Gamma}\widehat{u}(\bar{\boldsymbol{\xi}}, s) = \begin{bmatrix} \widehat{\mathcal{H}}(\bar{\boldsymbol{\xi}}, s) \\ \widehat{h}(\bar{\boldsymbol{\xi}}, s) \end{bmatrix}$$

where $\widehat{\mathcal{H}}$ and $\widehat{h}$ collect the values at interior and boundary collocation points, respectively. In the final step, the inverse Laplace transform is used to obtain the solution of Eqs (1.1)–(1.3).

1.2.3. Error analysis

The interpolation operator is based on Chebyshev collocation points Eq (1.7) and Lagrange polynomials Eq (1.6) as follows:

$$\mathcal{I}_m : C(\Gamma) \to \mathbb{P}_m, \quad \mathcal{I}_m(u) = \sum_{j=0}^{m} u(\xi_j)\eta_j(\xi).$$

The steps proposed in [50] will be followed for the construction of the interpolation polynomial error bound, for a constant $\mathcal{M}_m$, which satisfies the following estimate

$$\|\mathcal{I}_m(u)\|_\infty \leq \mathcal{M}_m\|u\|_\infty, \quad \forall\, u \in C[-1, 1] \tag{1.8}$$

Additionally,

$$\mathcal{I}_m(u) = u, \quad \forall \;\; u \in \mathbb{P}_m$$

It is possible to show that for Chebyshev interpolation,

$$\mathcal{M}_m = \frac{\ln(1+m)}{\frac{\pi}{2}} + 1 \leq (m+1)$$

Based on m, the constant of stability increases very slowly. For $u \in C^{m+1}[-1, 1]$, we have the following bound [50]

$$\|u - \mathcal{I}_m(u)\|_\infty \leq \frac{1}{2^m\Gamma(m+2)}\|u^{(m+1)}\|_\infty \tag{1.9}$$

Theorem 1. [50] If Eqs (1.8) and (1.9) hold, and $u \in C^{m+1}[-1, 1]$, we have

$$\|u^{(\ell)} - \mathcal{I}_m(u)^{(\ell)}\|_\infty \leq \frac{2^{(\ell-m)}(\mathcal{M}_m^{(\ell)}+1)}{\Gamma(m-\ell+2)}\|u^{(m+1)}\|_\infty, \; \ell = 0, 1, 2, ..., m \tag{1.10}$$

with the stability constant

$$\mathcal{M}_m^{(\ell)} = \frac{1}{\Gamma(\ell+1)}\left[\frac{\mathcal{M}_m\Gamma(m+1)}{\Gamma(m-\ell+1)}\right]$$

Proof: By using Eqs (1.9) and (1.10) for Eq (1.1) in the one-dimension case, the governing operator is written as $\mathcal{L} = \frac{\partial^2}{\partial \xi^2}$; thus, the error estimate is given as

$$\begin{aligned}
\mathbf{E} &= \Bigg\|\Bigg(\sum_{k=1}^{p} \varrho_{1,k} D_t^{\alpha_k} u + \varrho_2 D_t u + \sum_{r=1}^{q} \varrho_{3,r} D_t^{\beta_r} u + \varrho_4 u - \varrho_5 \mathcal{L}u - \varrho_6 D_t^{\gamma}(\mathcal{L}u)\Bigg) - \Bigg(\sum_{k=1}^{p} \varrho_{1,k} D_t^{\alpha_k} \mathcal{I}_m(u) \\
&+ \varrho_2 \mathcal{I}_m(D_t u) + \sum_{r=1}^{q} \varrho_{3,r} D_t^{\beta_r} \mathcal{I}_m(u) + \varrho_4 \mathcal{I}_m(u) - \varrho_5 \mathcal{L}\mathcal{I}_m(u) - \varrho_6 D_t^{\gamma}(\mathcal{L}\mathcal{I}_m(u))\Bigg)\Bigg\|_{\infty} \\
&= \Bigg\| \sum_{k=1}^{p} \varrho_{1,k} D_t^{\alpha_k}(u - \mathcal{I}_m(u)) + \varrho_2(D_t(u - \mathcal{I}_m(u))) + \sum_{r=1}^{q} \varrho_{3,r} D_t^{\beta_r}(u - \mathcal{I}_m(u)) \\
&+ \varrho_4(u - \mathcal{I}_m(u)) - \varrho_5 \mathcal{L}(u - \mathcal{I}_m(u)) - \varrho_6 D_t^{\gamma}(\mathcal{L}(u - \mathcal{I}_m(u)))\Bigg\|_{\infty} \\
&\le \Bigg\| \sum_{k=1}^{p} \varrho_{1,k} D_t^{\alpha_k}(u - \mathcal{I}_m(u))\Bigg\|_{\infty} + \Bigg\|\varrho_2 D_t(u - \mathcal{I}_m(u))\Bigg\|_{\infty} + \Bigg\| \sum_{r=1}^{q} \varrho_{3,r} D_t^{\beta_r}(u - \mathcal{I}_m(u))\Bigg\|_{\infty} \\
&+ \Bigg\|\varrho_4(u - \mathcal{I}_m(u))\Bigg\|_{\infty} + \Bigg\|\varrho_5 \mathcal{L}(u - \mathcal{I}_m(u))\Bigg\|_{\infty} + \Bigg\|\varrho_6 D_t^{\gamma}(\mathcal{L}(u - \mathcal{I}_m(u)))\Bigg\|_{\infty} \\
&\le \sum_{k=1}^{p} |\varrho_{1,k}| \|D_t^{\alpha_k}(u - \mathcal{I}_m(u))\|_{\infty} + |\varrho_2| \|D_t(u - \mathcal{I}_m(u))\|_{\infty} + \sum_{r=1}^{q} |\varrho_{3,r}| \|D_t^{\beta_r}(u - \mathcal{I}_m(u))\|_{\infty} \\
&+ |\varrho_4| \|u - \mathcal{I}_m(u)\|_{\infty} + |\varrho_5| \|u_{\xi\xi} - \mathcal{I}_m(u)_{\xi\xi}\|_{\infty} + |\varrho_6| \|D_t^{\gamma}(u_{\xi\xi} - \mathcal{I}_m(u)_{\xi\xi})\|_{\infty} \\
\mathbf{E} &\le \sum_{k=1}^{p} |\varrho_{1,k}| \|D_t^{\alpha_k}(u - \mathcal{I}_m(u))\|_{\infty} + |\varrho_2| \|D_t(u - \mathcal{I}_m(u))\|_{\infty} + \sum_{r=1}^{q} |\varrho_{3,r}| \|D_t^{\beta_r}(u - \mathcal{I}_m(u))\|_{\infty} \\
&+ |\varrho_4| \frac{1}{2^m \Gamma(m+2)} \|u^{(m+1)}\|_{\infty} + |\varrho_5| \frac{2(\mathcal{M}_m^{(2)} + 1)}{\Gamma(m)} \left(\frac{1}{2}\right)^{m-1} \|u^{(m+1)}\|_{\infty} + |\varrho_6| \|D_t^{\gamma}(u_{\xi\xi} - \mathcal{I}_m(u)_{\xi\xi})\|_{\infty}
\end{aligned}$$

since the time derivatives are accurately computed. Therefore, the error bound of $\|D_t^{\alpha}(u - \mathcal{I}_m(u))\|_{\infty}, \|D_t(u - \mathcal{I}_m(u))\|_{\infty}, \|D_t^{\beta}(u - \mathcal{I}_m(u))\|_{\infty}$ and $\|u - \mathcal{I}_m(u)\|_{\infty}$ are of the same order and the error bound of $\|D_t^{\gamma}(u_{\xi\xi} - \mathcal{I}_m(u)_{\xi\xi})\|_{\infty}$ and $\|u_{\xi\xi} - \mathcal{I}_m(u)_{\xi\xi}\|_{\infty}$ are of the same order. Thus, the following stability bound is obtained:

$$\mathbf{E} \le \mathcal{N} \|u^{(m+1)}\|_{\infty}$$

where the constant $\mathcal{N}$ is determined by computing the coefficients of $\|u^{(m+1)}\|_{\infty}$. A similar stability estimate can be obtained for two-dimensional problems by using the tensor product interpolation operators.

1.3. Inversion of Laplace transform

In this section, we utilize numerical inverse Laplace methods to transform the pseudospectral method solution $\widehat{u}(\bar{\boldsymbol{\xi}}, s)$ from the Laplace domain to the time domain $u(\bar{\boldsymbol{\xi}}, t)$ as follows:

$$u(\bar{\boldsymbol{\xi}}, t) = \frac{1}{2\pi i} \int_{\rho - i\infty}^{\rho + i\infty} e^{s\tau} \widehat{u}(\bar{\boldsymbol{\xi}}, s) ds, \ \rho > \rho_0 \tag{1.11}$$

Here, $\widehat{u}(\bar{\boldsymbol{\xi}}, s)$ needs to be inverted and the converging abscissa is ρ_0 and $\rho > \rho_0$. Thus, the open half plane $Re(s) < \rho$ contains all the singularities of $\widehat{u}(\bar{\boldsymbol{\xi}}, s)$. Our goal is to approximate the integral defined in Eq (1.11). In most cases, the integral defined in Eq (1.11) is quite difficult to be evaluated analytically; therefore, a numerical method needs to be employed. The integral defined in Eq (1.11) may be evaluated by several numerical algorithms available in literature. Every approach has a distinct application and is appropriate for a certain type of function. In this article, we use the two popular inversion algorithms, the improved Talbot's method [51] and the Stehfest's method [52], which are presented as follows.

1.3.1. Talbot's method

Here, we utilize the Talbot's method to approximate $u(\bar{\boldsymbol{\xi}}, t)$

$$u(\bar{\boldsymbol{\xi}}, t) = \frac{1}{2\pi i}\int_{\rho-i\infty}^{\rho+i\infty} e^{st}\widehat{u}(\bar{\boldsymbol{\xi}}, s)ds = \frac{1}{2\pi i}\int_{\Lambda} e^{st}\widehat{u}(\bar{\boldsymbol{\xi}}, s)ds,\ Re(s) > 0 \tag{1.12}$$

where Λ is a suitably chosen contour. In the Talbot's method, the numerical quadrature is applied to the integral in Eq (1.12). The trapezoidal and midpoint rule are the two effective rules used in conjunction with the deformation of contour [53]. The purpose of contour deformation is to handle the exponential factor. Particularly, the path of integration can be deformed to a Hankel contour, i.e., a contour whose real part starts at $-\infty$ in the 3rd quadrant and winds around all the singularities of the transform function going again to $-\infty$ in the 2nd quadrant. The exponential component decays rapidly on such contour, making the Bromwich integral appropriate for approximation and using the trapezoidal and midpoint rule. Cauchy's theorem justifies such deformation, provided that the contour remains in the region where the transformed function $\widehat{u}(\bar{\boldsymbol{\xi}}, s)$ is analytic. Furthermore, some mild restrictions are required in the left complex plane on the decay of the transformed function $\widehat{u}(\bar{\boldsymbol{\xi}}, s)$ [54, 55]. We consider the contour in the following parametric form as [51]

$$\Lambda : s = s(\omega), \quad -\pi \leq \omega \leq \pi,\ Res(\pm\pi) = -\infty$$

We have

$$s(\omega) = \frac{m_T}{t}\varpi(\omega),\ \varpi(\omega) = -\eta_1 + \eta_2\omega\cot(\eta_3\omega) + \eta_4 i\omega \tag{1.13}$$

where $\eta_1,\ \eta_2,\ \eta_3$, and η_4 are to be selected by the user. Plugging Eq (1.13) in Eq (1.12), we have

$$u(\bar{\boldsymbol{\xi}}, t) = \frac{1}{2\pi i}\int_{-\pi}^{\pi} e^{s(\omega)t}\widehat{u}(\bar{\boldsymbol{\xi}}, s)(s(\omega))s'(\omega)d\omega \tag{1.14}$$

Midpoint rule with uniform step $h = \frac{2\pi}{m_T}$ is utilized to approximate Eq (1.14) as

$$u_{App}(\bar{\boldsymbol{\xi}}, t) \approx \frac{1}{m_T i}\sum_{k=1}^{m_T} e^{s(\omega_k)t}\widehat{u}(s(\omega_k))s'(\omega_k), \quad \omega_k = -\pi + (k - \frac{1}{2})h \tag{1.15}$$

1.3.2. Error analysis

The error analysis of the improved Talbot's approach is based on the following theorem.

Theorem 1.1. [51] Let ω_k be defined as in Eq (1.15). Let $g : \Xi \to \mathbb{C}$ be an analytic function in the set

$$\Xi = \{\omega \in \mathbb{C} : -\pi < Re\omega < \pi, \text{and} - s < Im\omega < r\}$$

when $r, s > 0$, then

$$\int_{-\pi}^{\pi} g(\omega)d\omega - \frac{2\pi}{m_T}\sum_{j=1}^{m_T} g(\omega_k) = \Psi_{-}(\phi) + \Psi_{+}(\psi)$$

where

$$\Psi_{+}(\phi) = \frac{1}{2}\left(\int_{-\pi}^{-\pi+i\phi} + \int_{-\pi+i\phi}^{\pi+i\phi} + \int_{\pi+i\phi}^{\pi}\right)\left(1 + i\tan\left(\frac{m_T\omega}{2}\right)\right)g(\omega)d\omega$$

and

$$\Psi_{-}(\psi) = \frac{1}{2}\left(\int_{-\pi}^{-\pi-i\psi} + \int_{-\pi-i\psi}^{\pi-i\psi} + \int_{\pi-i\psi}^{\pi}\right)\left(1 - i\tan\left(\frac{m_T\omega}{2}\right)\right)g(\omega)d\omega$$

$\forall\ 0 < \phi < r,\ 0 < \psi < s,$ and m_T even if m_T is an odd number; we can replace $\tan(\frac{m_T\omega}{2})$ with $-\cot(\frac{m_T\omega}{2})$ if $g(\omega)$ is real valued, that is, $g(\bar{\omega}) = \overline{g(\omega)}$ and if r and s can be taken to be equal, then

$$\Psi(\psi) = \Psi_{+}(\psi) + \Psi_{-}(\psi) = Re\int_{-\pi+i\psi}^{\pi+i\psi}\left(1 + i\tan\left(\frac{m_T\omega}{2}\right)\right)g(\omega)d\omega$$

By examining the complex tangent function's behavior, this may be bounded as

$$|\Psi(\psi)| \leq \frac{4\pi C}{exp(rm_T) - 1}$$

The above process has been done for even m_T and C and r are some positive constants. A similar approach can be used for an odd m_T.

The optimal values of the parameters included in Eq (1.13) can be utilized to find the optimal contour of integration, which is necessary to obtain the best results. The authors of [51] have obtained the optimal values of the parameters as follows

$$\eta_1 = 0.61220,\ \eta_2 = 0.50170,\ \eta_3 = 0.64070, \text{and}\ \eta_4 = 0.26450$$

The corresponding error estimate is given as

$$Err_{est} = |\ u_{App}(\bar{\boldsymbol{\xi}}, t) - u(\bar{\boldsymbol{\xi}}, t)| = \mathbf{O}(e^{(-1.358)m_T})$$

1.4. Stehfest's method

One of the most effective and straightforward techniques for Laplace transform inversion is the Gaver-Stehfest approach. The latter part of the 1960s saw its design. Because of its simplicity and efficacy, it has become more and more popular in a variety of fields, including computational physics, finance, economics, and chemistry. The basis of the Gaver-Stehfest approach is the series of Gaver approximants, as found by Gaver [56]. Since the convergence of the Gaver approximants was essentially logarithmic, acceleration was necessary. A linear acceleration approach was provided by Stehfest [52] using the Salzer acceleration method. Using a series of functions, the Gaver-Stehfest method approximates $u(\bar{\boldsymbol{\xi}}, t)$ as

$$u_{App}(\bar{\boldsymbol{\xi}}, t) = \frac{\ln 2}{t}\sum_{k=1}^{m_S}\theta_k\widehat{u}\left(\bar{\boldsymbol{\xi}}, \frac{\ln 2}{t}k\right) \tag{1.16}$$

where θ_k are given as

$$\theta_k = (-1)^{\frac{m_S}{2}+k} \sum_{n=\lfloor \frac{k+1}{2} \rfloor}^{min(k,\frac{m_S}{2})} \frac{n^{\frac{m_S}{2}}(2n)!}{(\frac{m_S}{2}-n)!n!(n-1)!(k-n)!(2n-k)!} \tag{1.17}$$

Solving the system Eqs (1.4) and (1.5) for the corresponding Laplace parameters $s = \frac{ln2}{t}k,\ k = 1,2,3,...,m_S$, the approximate solution $u_{App}(\bar{\xi},t)$ of the problem in Eq (1.1) can be obtained via Eq (1.16). The Gaver-Stehfest algorithm has a few noteworthy qualities, such as: (i) $u(\bar{\xi},t)$ are linear in the context of values of $\widehat{u}(\bar{\xi},s)$; (ii) the values of $\widehat{u}(\bar{\xi},s)$ are required merely for real value of s; (iii) the procedure of determining the coefficients is fairly effortless; (iv) for constant functions, this approach results in significantly precise approximations, i.e., if $u \equiv c$, then $u_{App} \equiv c$ for all $m_S \geq 1$. In literature, this methodology has been employed by many researchers in [57, 58], in which it is revealed that this strategy converges promptly to $u_{App}(\bar{\xi},t)$ (given $u(\bar{\xi},t)$ is non-oscillatory).

Convergence

The convergence of $u_{App}(\bar{\xi},t)$ has been derived by the author in [57]. The results are based on the following theorem.

Theorem 1.2. *Let $u : (0,\infty) \to \mathbb{R}$ be a locally integrable function. Let $s > 0$, define the Laplace transform $\widehat{u}(\bar{\xi},s)$, and let $u_{App}(\bar{\xi},t)$ be the numerical solution as given by Eq* (1.16).

1. *$u_{App}(\bar{\xi},t)$ converges given $u(\bar{\xi},t)$ near t.*
2. *Let for some real number ϕ and $0 < \psi < 0.25$,*

$$\int_0^{\psi} |u(\bar{\xi},-t\log_2(1/2+\eta)) + u(\bar{\xi},-t\log_2(1/2-\eta)) - 2\phi|\eta^{-1}d\eta < \infty$$

   then $u_{App}(\bar{\xi},t) \to \phi$ as $m_S \to +\infty$.
3. *Let $u(\bar{\xi},t)$ be of bounded variation near t, then*

$$u_{App}(\bar{\xi},t) \to \frac{u(\bar{\xi},t+0)+u(\bar{\xi},t-0)}{2},\ as\ m_S \to +\infty$$

Corollary 1.3. *Using the assumptions of the above theorem, if*

$$u(\bar{\xi},t+\eta) - u(\bar{\xi},t) = O\left(|\eta|^{\vartheta}\right)$$

$\forall\ \eta$, and some ϑ, then $u_{App}(\bar{\xi},t) \to u(\bar{\xi},t)$ as $m_S \to +\infty$.

Moreover, the authors in [59] conducted a number of experiments to determine how parameters affected the numerical scheme's correctness. Their conclusions are as follows: "For ν_1 significant digits, select a m_S positive integer $\lceil 2.2\nu_1 \rceil$: After setting the system precision to $\nu_2 = \lceil 1.1 m_S \rceil$, compute $\theta_i, 1 \leq i \leq m_S$ for a given m_S using Eq (1.17). Next, compute the $u_{App}(\bar{\xi},t)$ in Eq (1.16) for the provided transformed function $\widehat{u}(\bar{\xi},s)$ and the argument t." These conclusions indicate that the error is $10^{-(\nu_1+1)} \leq \frac{u_{App}(\bar{\xi},t)-u(\bar{\xi},t)}{u(\bar{\xi},t)} \leq 10^{-\nu_1}$, where $m_S = \lceil 2.2\nu_1 \rceil$ [40].

2. Application

In this section, three test problems are considered to assess the effectiveness and accuracy of the Laplace transformed pseudospectral method. We compute the maximum absolute error (Err_∞), the relative error (Err_2), and the root mean square error (Err_{rms}) between the numerical and the exact solutions, which are defined as follows:

$$Err_\infty = \max_{1\le k\le m} |u(\bar{\boldsymbol{\xi}}_k, t) - u_{App}(\bar{\boldsymbol{\xi}}_k, t)|,$$

$$Err_2 = \sqrt{\frac{\sum_{k=1}^{m}(u(\bar{\boldsymbol{\xi}}_k, t) - u_{App}(\bar{\boldsymbol{\xi}}_k, t))^2}{\sum_{k=1}^{m}(u(\bar{\boldsymbol{\xi}}_k, t))^2}},$$

$$Err_{rms} = \sqrt{\frac{\sum_{k=1}^{m}(u(\bar{\boldsymbol{\xi}}_k, t) - u_{App}(\bar{\boldsymbol{\xi}}_k, t))^2}{m}}$$

where $u_{App}(\bar{\boldsymbol{\xi}}_k, t)$ is the approximate solution and $u(\bar{\boldsymbol{\xi}}_k, t)$ is the exact solution.

Problem 1

We consider Eq (1.1) with exact solution

$$u(\xi, \zeta, t) = (t^3 + 1)\sin(\pi\xi)\sin(\pi\zeta)$$

and the source term is

$$\mathcal{G}(\xi, \zeta, t) = \sin(\pi\xi)\sin(\pi\zeta)\Big[\varrho_{1,1}\frac{6}{\Gamma(4-\alpha)}t^{3-\alpha} + 3\varrho_2 t^2 + \varrho_{3,1}\frac{6}{\Gamma(4-\beta)}t^{3-\beta} + (\varrho_4 + 2\varrho_5\pi^2)(t^3+1) + 2\varrho_6\pi^2\frac{6}{\Gamma(4-\gamma)}t^{3-\gamma}\Big]$$

where $\varrho_{1,1} = \varrho_2 = \varrho_{3,1} = \varrho_4 = \varrho_5 = \varrho_6 = 1$ and $(\xi, \zeta) \in [-1, 1]^2$. The initial-boundary conditions are obtained from the analytical solution. The Err_2, Err_∞, and Err_{rms} errors of the proposed method for problem 1 obtained via the Stehfest's and the Talbot's methods by using various values of m, m_T, m_S, α, β, γ, and $t = 1$ are presented in Tables 1 and 2, respectively. The numerical solution to problem 1 is shown in Figure 1. Figure 2 presents a comparison of error norms Err_2, Err_∞, and Err_{rms} computed using the Stehfest's and the Talbot's methods for various values of m_S and m_T with $\alpha = 1.5$, $\beta = 0.7$, $\gamma = 0.3$, $m = 30$, and $t = 1$. The comparison of Err_2, Err_∞, and Err_{rms} computed by the Stehfest's and the Talbot's methods for different values of t with $\alpha = 1.5$, $\beta = 0.7$, $\gamma = 0.3$, $m_S = 14$, $m_T = 30$, and $m = 30$ is shown in Figure 3. The comparison of Err_2, Err_∞, and Err_{rms} computed using the Stehfest's and the Talbot's methods versus α with $\beta = 0.7$, $\gamma = 0.3$, $m = 30$, $m_S = 14$, $m_T = 30$, and $t = 1$ is presented in Figure 4. The comparison of Err_2, Err_∞, and Err_{rms} computed via the Stehfest's and the Talbot's methods versus β with $\alpha = 1.5, \gamma = 0.7, m = 30, m_S = 14, m_T = 30$, and $t = 1$ is presented in Figure5. The comparison of Err_2, Err_∞, and Err_{rms} computing by the Stehfest's and the Talbot's methods versus γ with $\alpha = 1.5, \beta = 0.7, m = 30, m_S = 14, m_T = 30$, and $t = 1$ is presented in Figure 6. The plot of Err_2

obtained via the Stehfest's and the Talbot's methods for $\alpha \in [1,2]$ and $\beta \in [0,1]$ with $\gamma = 0.3,\ t = 1,\ m_S = 16, m_T = 30$, and $m = 30$ is shown in Figure 7. In Figure 8, the plots of Err_∞ obtained using the Stehfest's and the Talbot's methods for $\alpha \in [1,2]$ and $\gamma \in [0,1]$ with $\beta = 0.7,\ t = 1,\ m_S = 16,\ m_T = 30$, and $m = 30$ are shown. Similarly, Figure 9 presents the plots of Err_{rms} obtained using the Stehfest's and the Talbot's methods for $\alpha \in [1,2]$ and $t \in [0,1]$ with $\beta = 0.7, \gamma = 0.3, m_S = 16,\ m_T = 30$, and $m = 30$. It is observed that the accuracy of the Stehfest's method steadily decreases for $m_S \geq 14$. From the results presented in tables and figures, we conclude that the proposed method is accurate, stable, and efficient. The numerical results demonstrate that the Talbot's method is more accurate than the Stehfest's method.

Table 1. The $Err_2, Err_\infty, Err_{rms}$ computed by the Stehfest's method for problem 1.

(α,β,γ)	m	m_S	Err_2	Err_∞	Err_{rms}	CPU (sec.)
$(1.3, 0.2, 0.9)$	22	14	4.7216×10^{-04}	9.6894×10^{-05}	2.1462×10^{-05}	0.199250
	25		5.3662×10^{-04}	1.0751×10^{-04}	2.1465×10^{-05}	0.326975
	28		7.5644×10^{-04}	1.0128×10^{-04}	2.7016×10^{-05}	0.556057
	30	10	6.9931×10^{-02}	5.9791×10^{-03}	2.3310×10^{-03}	0.575029
		12	1.5653×10^{-03}	1.3408×10^{-04}	5.2178×10^{-05}	0.663883
		14	7.8051×10^{-04}	1.3790×10^{-04}	2.6017×10^{-05}	0.755536
$(1.6, 0.5, 0.7)$	22	14	4.0428×10^{-04}	4.4012×10^{-05}	1.8376×10^{-05}	0.180055
	25		4.8390×10^{-04}	4.4246×10^{-05}	1.9356×10^{-05}	0.324530
	28		6.4225×10^{-04}	8.5592×10^{-05}	2.2938×10^{-05}	0.576450
	30	10	6.9931×10^{-02}	5.9791×10^{-03}	2.3310×10^{-03}	0.581491
		12	1.5680×10^{-03}	1.3409×10^{-04}	5.2266×10^{-05}	0.688463
		14	7.4051×10^{-04}	1.3304×10^{-04}	2.4684×10^{-05}	0.719391
$(1.9, 0.8, 0.5)$	22	14	3.8530×10^{-04}	4.2171×10^{-05}	1.7514×10^{-05}	0.184399
	25		4.5504×10^{-04}	4.3708×10^{-05}	1.8202×10^{-05}	0.329158
	28		5.2746×10^{-04}	6.0001×10^{-05}	1.8838×10^{-05}	0.556485
	30	10	6.9931×10^{-02}	5.9791×10^{-03}	2.3310×10^{-03}	0.514627
		12	1.5660×10^{-03}	1.3402×10^{-04}	5.2201×10^{-05}	0.630183
		14	6.5840×10^{-04}	1.3505×10^{-04}	2.1947×10^{-05}	0.760430

Table 2. The $Err_2, Err_\infty, Err_{rms}$ computed by the Talbot's method for problem 1.

(α,β,γ)	m	m_T	Err_2	Err_∞	Err_{rms}	CPU (sec.)
$(1.3, 0.2, 0.9)$	22	30	1.4423×10^{-10}	3.8758×10^{-11}	6.5561×10^{-12}	1.431363
	25		2.2738×10^{-10}	6.1642×10^{-11}	9.0953×10^{-12}	2.823492
	28		3.0634×10^{-10}	5.6744×10^{-11}	1.0941×10^{-11}	4.853607
	30	20	5.1049×10^{-06}	4.3647×10^{-07}	1.7016×10^{-07}	4.409938
		25	1.1297×10^{-08}	9.6706×10^{-10}	3.7658×10^{-10}	5.576429
		30	3.7908×10^{-10}	8.4039×10^{-11}	1.2636×10^{-11}	6.435613
$(1.6, 0.5, 0.7)$	22	30	8.8800×10^{-11}	1.6472×10^{-11}	4.0364×10^{-12}	1.432723
	25		1.3312×10^{-10}	3.5030×10^{-11}	5.3248×10^{-12}	2.644643
	28		1.9449×10^{-10}	3.9329×10^{-11}	6.9462×10^{-12}	4.498548
	30	20	5.1049×10^{-06}	4.3647×10^{-07}	1.7016×10^{-07}	4.512210
		25	1.1277×10^{-08}	9.6519×10^{-10}	3.7589×10^{-10}	5.250997
		30	2.5877×10^{-10}	8.3971×10^{-11}	8.6256×10^{-12}	6.315079
$(1.9, 0.8, 0.5)$	22	30	6.3703×10^{-11}	1.7695×10^{-11}	2.8956×10^{-12}	1.465253
	25		9.4756×10^{-11}	2.4410×10^{-11}	3.7902×10^{-12}	2.624655
	28		1.5070×10^{-10}	5.0718×10^{-11}	5.3821×10^{-12}	4.675835
	30	20	5.1049×10^{-06}	4.3647×10^{-07}	1.7016×10^{-07}	4.469602
		25	1.1281×10^{-08}	9.6487×10^{-10}	3.7602×10^{-10}	5.300393
		30	2.0811×10^{-10}	4.6520×10^{-11}	6.9370×10^{-12}	6.311030

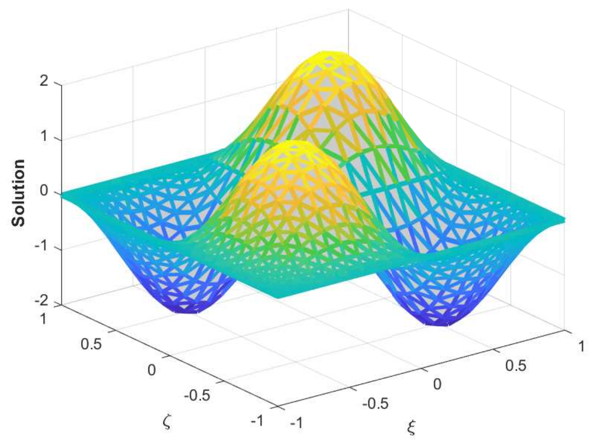

Figure 1. Numerical solution of problem 1 obtained by proposed scheme.

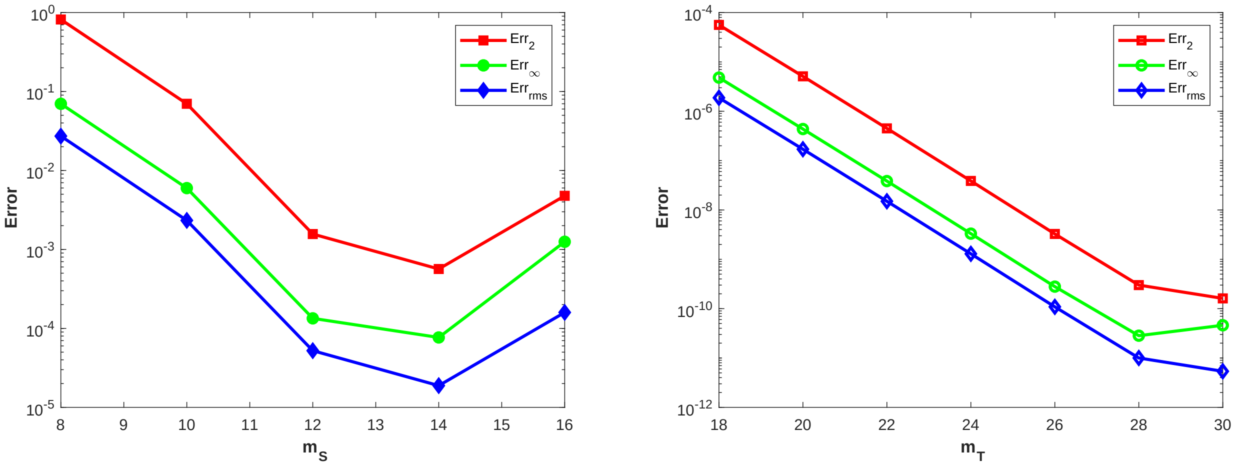

(a) (b)

Figure 2. (a) Plots of Err_2, Err_∞, and Err_{rms} obtained by Stehfest's method versus m_S and for $\alpha = 1.5, \beta = 0.7, \gamma = 0.3, t = 1$, and $m = 30$. (b) Plots of Err_2, Err_∞, and Err_{rms} obtained by Talbot's method versus m_T for $\alpha = 1.5, \beta = 0.7, \gamma = 0.3, t = 1$, and $m = 30$.

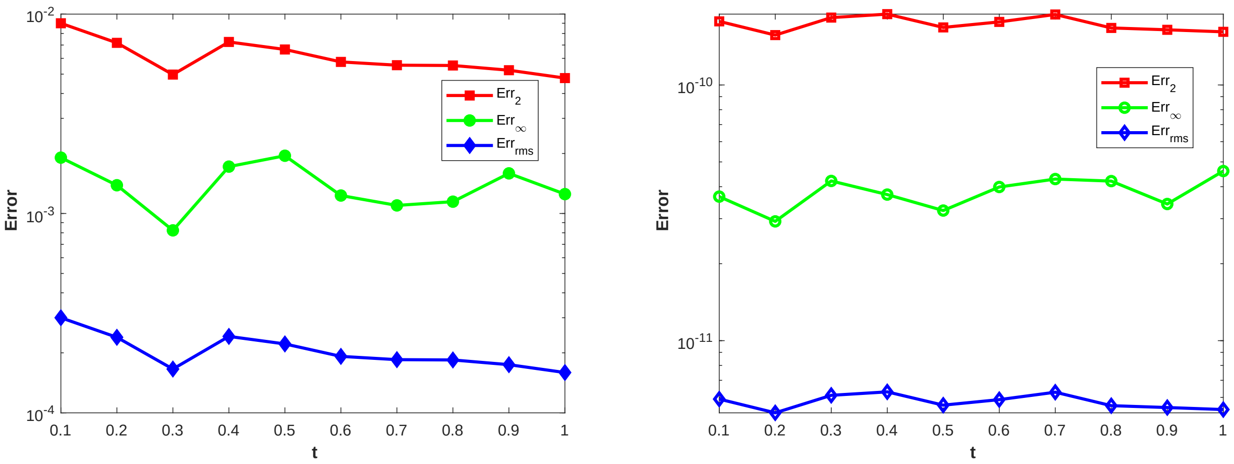

(a) (b)

Figure 3. (a) Plots of Err_2, Err_∞, and Err_{rms} obtained by Stehfest's method versus t for $\alpha = 1.5$, $\beta = 0.7$, $\gamma = 0.3$, $m_S = 14$, and $m = 30$. (b) Plots of Err_2, Err_∞, and Err_{rms} obtained by Talbot's method versus t for $\alpha = 1.5$, $\beta = 0.7$, $\gamma = 0.3$, $m_T = 30$, and $m = 30$.

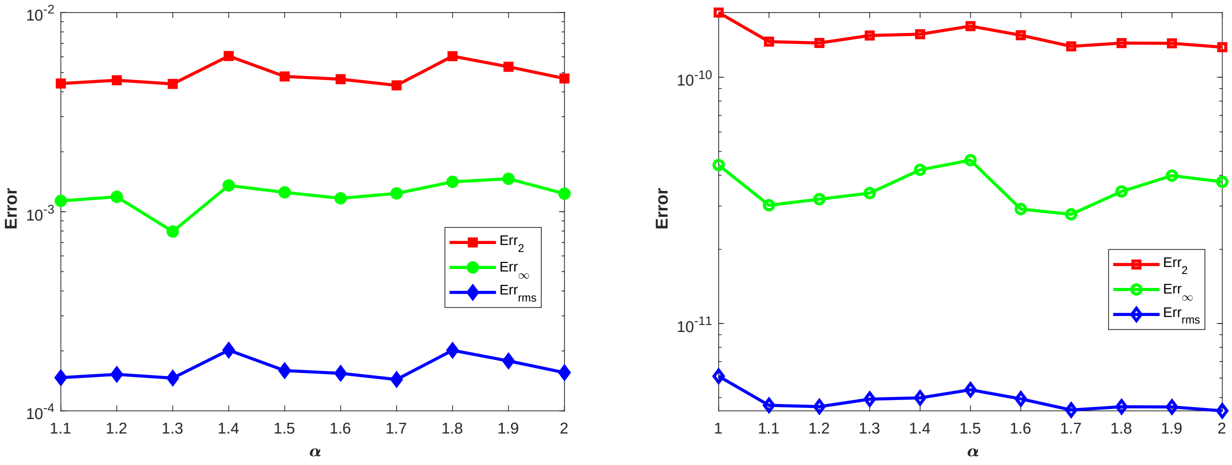

(a) **(b)**

Figure 4. (a) Plots of Err_2, Err_∞, and Err_{rms} obtained by Stehfest's method versus α for $\beta = 0.7,\ \gamma = 0.3,\ m_S = 14,\ t = 1$, and $m = 30$. (b) Plots of Err_2, Err_∞, and Err_{rms} obtained by Talbot's method versus α for $\beta = 0.7,\ \gamma = 0.3,\ m_T = 30,\ t = 1$, and $m = 30$.

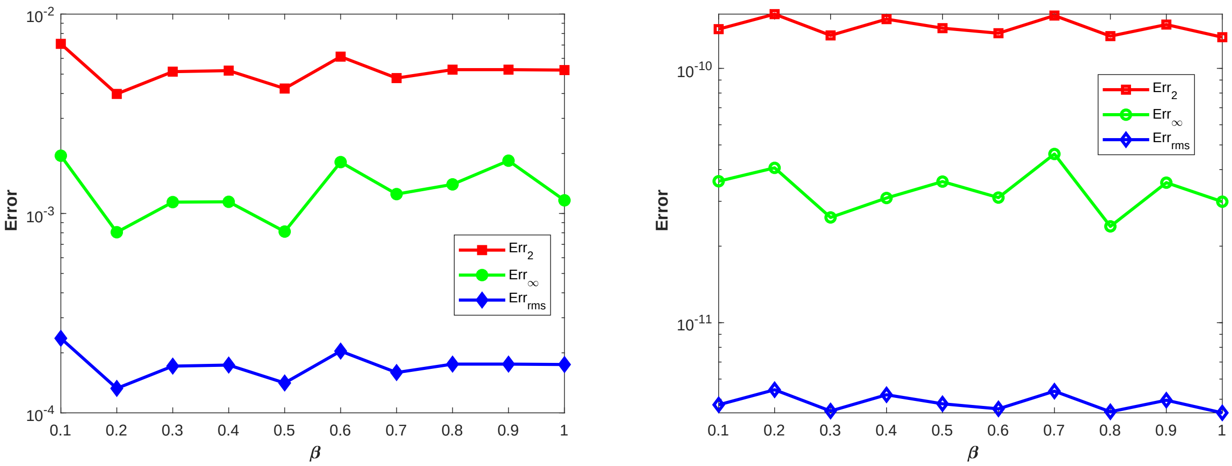

(a) **(b)**

Figure 5. (a) Plots of Err_2, Err_∞, and Err_{rms} obtained by Stehfest's method versus β for $\alpha = 1.5,\ \gamma = 0.3,\ m_S = 14,\ t = 1$, and $m = 30$. (b) Plots of Err_2, Err_∞, and Err_{rms} obtained by Talbot's method versus β for $\alpha = 1.5,\ \gamma = 0.3,\ m_T = 30,\ t = 1$, and $m = 30$.

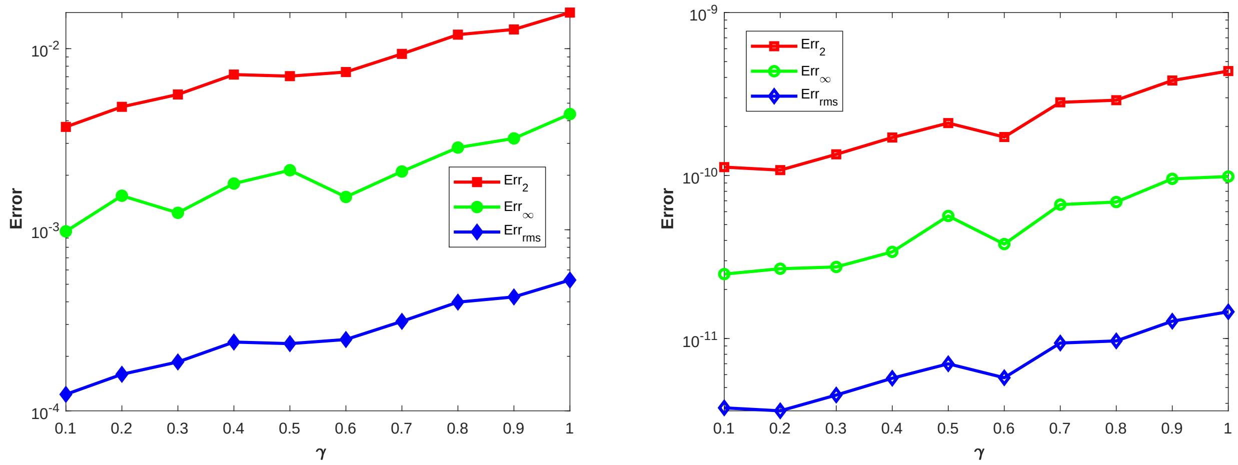

(a) **(b)**

Figure 6. (a) Plots of Err_2, Err_∞, and Err_{rms} versus γ obtained by Stehfest's method for $\alpha = 1.5,\ \beta = 0.7,\ m_S = 14,\ t = 1$, and $m = 30$. (b) Plots of Err_2, Err_∞, and Err_{rms} versus γ obtained by Talbot's method for $\alpha = 1.5,\ \beta = 0.7,\ m_T = 30,\ t = 1$, and $m = 30$.

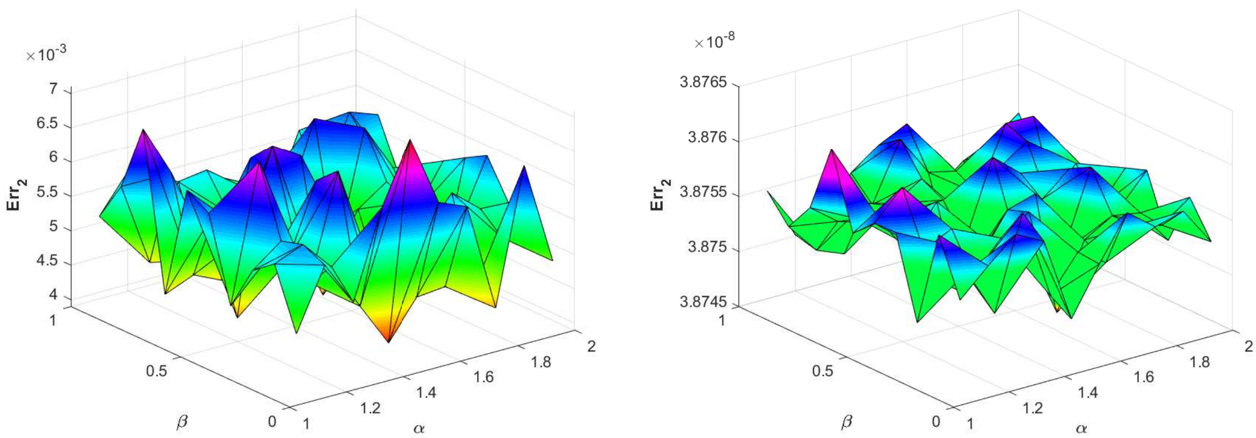

(a) **(b)**

Figure 7. (a) Plot of Err_2 versus α and β obtained by Stehfest's method for $\gamma = 0.3,\ t = 1,\ m_S = 16$, and $m = 30$. (b) Plot of Err_2 versus α and β obtained by Talbot's method for $\gamma = 0.3,\ t = 1,\ m_T = 24$, and $m = 30$.

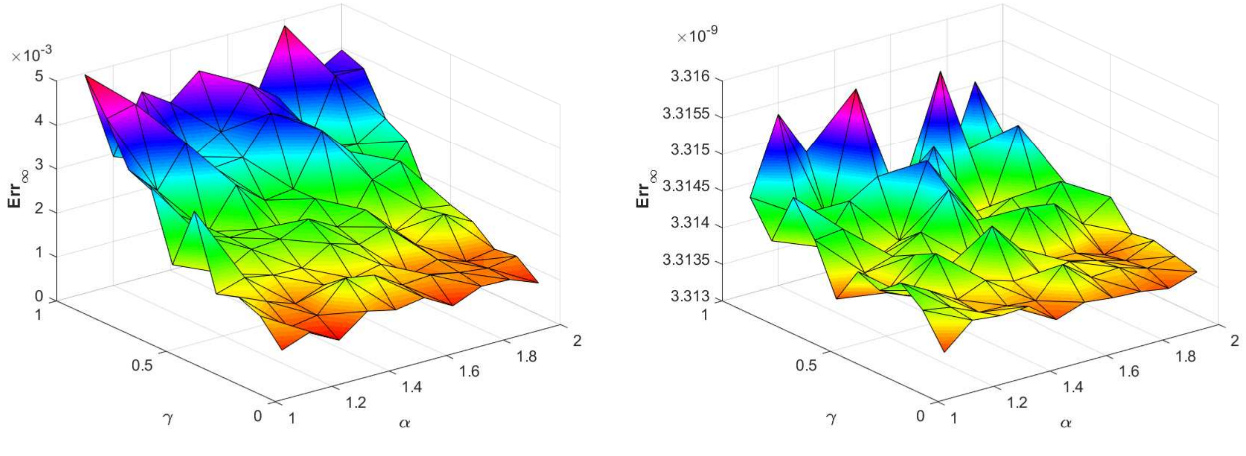

(a) **(b)**

Figure 8. (a) Plot of Err_∞ versus α and γ obtained by Stehfest's method for $\beta = 0.7,\ t = 1,\ m_S = 16$, and $m = 30$. (b) Plot of Err_∞ versus α and γ obtained by Talbot's method for $\beta = 0.7,\ t = 1,\ m_T = 24$, and $m = 30$.

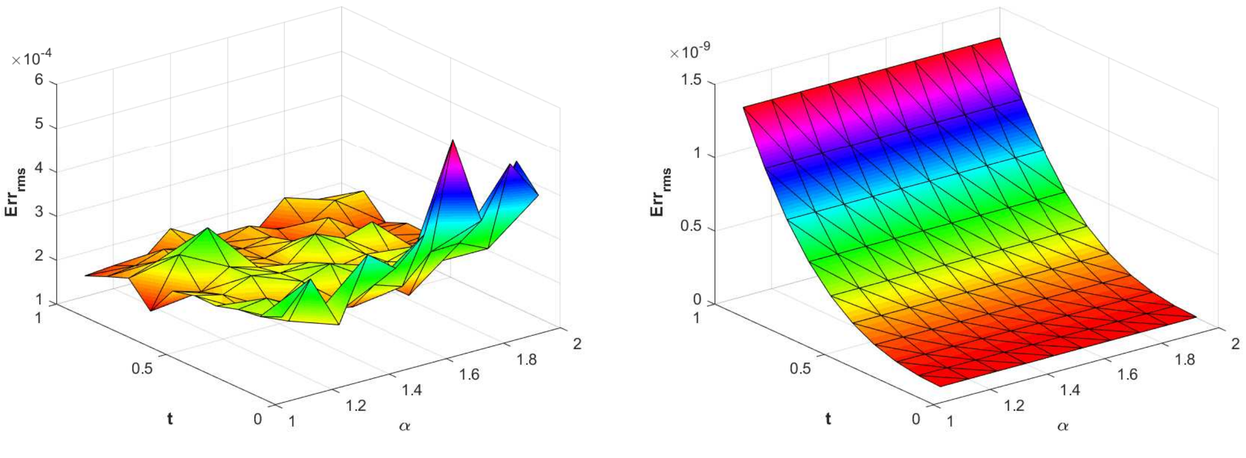

(a) **(b)**

Figure 9. (a) Plot of Err_{rms} versus α and t obtained by Stehfest's method for $\beta = 0.7,\ \gamma = 0.3,\ m_S = 16$, and $m = 30$. (b) Plot of Err_{rms} versus α and t obtained by Talbot's method for $\beta = 0.7,\ \gamma = 0.3,\ m_T = 24$, and $m = 30$.

Problem 2

We consider Eq (1.1) with exact solution

$$u(\xi,\zeta,t) = (t^3+1)(1-\xi^2-\zeta^2)$$

and the source term is

$$\begin{aligned}\mathcal{G}(\xi,\zeta,t) =&(1-\xi^2-\zeta^2)\Big[\varrho_{1,1}\frac{6}{\Gamma(4-\alpha)}t^{3-\alpha}+3\varrho_2 t^2+\varrho_{3,1}\frac{6}{\Gamma(4-\beta)}t^{3-\beta}\\ &+\varrho_4(t^3+1)\Big]+4\varrho_5(t^3+1)+\varrho_6\frac{6}{\Gamma(4-\gamma)}t^{3-\gamma}\end{aligned}$$

where $\varrho_{1,1} = \varrho_2 = \varrho_{3,1} = \varrho_4 = \varrho_5 = \varrho_6 = 1$, $(\xi,\zeta) \in [-1,1]^2$ and the initial-boundary conditions are obtained from the analytical solution.

The Err_2, Err_∞, and Err_{rms} errors of the proposed method for problem 2 obtained via the Stehfest's and the Talbot's methods by using various values of m, m_T, m_S, α, β, γ, and $t = 1$ are presented in Tables 3 and 4, respectively.

The numerical solution of problem 2 is shown in Figure 10. Figure 11 presents a comparison of error norms Err_2, Err_∞, and Err_{rms} computed via the Stehfest's and the Talbot's methods versus m_S and m_T with $\alpha = 1.5$, $\beta = 0.7$, $\gamma = 0.3$, $m = 30$, and $t = 1$. The comparison of Err_2, Err_∞, and Err_{rms} obtained using the Stehfest's and the Talbot's methods versus t with $\alpha = 1.5$, $\beta = 0.7$, $\gamma = 0.3$, $m_S = 14$, $m_T = 30$, and $m = 30$ is shown in Figure 12.

The comparison of Err_2, Err_∞, and Err_{rms} obtained using the Stehfest's and the Talbot's methods versus α with $\beta = 0.7$, $\gamma = 0.3$, $m = 30$, $m_S = 14$, $m_T = 30$, and $t = 1$ is presented in Figure 13. The comparison of Err_2, Err_∞, and Err_{rms} computed using the Stehfest's and the Talbot's methods versus β with $\alpha = 1.5, \gamma = 0.7, m = 30, m_S = 14, m_T = 30$, and $t = 1$ is shown in Figure 14.

The comparison of Err_2, Err_∞, and Err_{rms} obtained using the Stehfest's and the Talbot's methods versus γ with $\alpha = 1.5, \beta = 0.7, m = 30, m_S = 14, m_T = 30$, and $t = 1$ is presented in Figure 15. The plots of Err_2 obtained using the Stehfest's and the Talbot's methods for $\alpha \in [1,2]$ and $\beta \in [0,1]$ with $\gamma = 0.3$, $t = 1$, $m_S = 16, m_T = 30$, and $m = 30$ are shown in Figure 16.

In Figure 17, the plots of Err_∞ obtained using the Stehfest's and the Talbot's methods for $\alpha \in [1,2]$ and $\gamma \in [0,1]$ with $\beta = 0.7$, $t = 1$, $m_S = 16$, $m_T = 30$, and $m = 30$ are shown. Similarly, Figure 18 shows the plot of Err_{rms} obtained via the Stehfest's and the Talbot's methods for $\alpha \in [1,2]$ and $t \in [0,1]$ with $\beta = 0.7, \gamma = 0.3, m_S = 16$, $m_T = 30$, and $m = 30$. Comparable performances like the one we witnessed in Problem 2 are observed.

Table 3. The $Err_2, Err_\infty, Err_{rms}$ computed by Stehfest's method for problem 2.

(α,β,γ)	m	m_S	Err_2	Err_∞	Err_{rms}	CPU (sec.)
$(1.3, 0.2, 0.9)$	22	14	4.4852×10^{-03}	1.6695×10^{-03}	2.0387×10^{-04}	0.188688
	25		6.8895×10^{-03}	1.5726×10^{-03}	2.7558×10^{-04}	0.394322
	28		1.7303×10^{-02}	6.2685×10^{-03}	6.1797×10^{-04}	0.524445
	30	10	9.4263×10^{-02}	5.9793×10^{-03}	3.1421×10^{-03}	0.568557
		12	2.1084×10^{-03}	3.2664×10^{-04}	7.0279×10^{-05}	0.658355
		14	2.4313×10^{-02}	9.5089×10^{-03}	8.1042×10^{-04}	0.818657
$(1.6, 0.5, 0.7)$	22	14	2.2303×10^{-03}	1.0201×10^{-03}	1.0138×10^{-04}	0.200221
	25		6.1739×10^{-03}	2.3026×10^{-03}	2.4695×10^{-04}	0.316503
	28		9.0251×10^{-03}	2.3816×10^{-03}	3.2232×10^{-04}	0.510553
	30	10	9.4257×10^{-02}	5.9791×10^{-03}	3.1419×10^{-03}	0.550572
		12	2.0884×10^{-03}	2.1157×10^{-04}	6.9612×10^{-05}	0.663605
		14	1.3078×10^{-02}	3.9249×10^{-03}	4.3594×10^{-04}	0.735535
$(1.9, 0.8, 0.5)$	22	14	1.7605×10^{-03}	4.8804×10^{-04}	8.0021×10^{-05}	0.181867
	25		3.2429×10^{-03}	1.5817×10^{-03}	1.2971×10^{-04}	0.318878
	28		7.1727×10^{-03}	2.6411×10^{-03}	2.5617×10^{-04}	0.512775
	30	10	9.4250×10^{-02}	5.9791×10^{-03}	3.1417×10^{-03}	0.585836
		12	2.1968×10^{-03}	2.7998×10^{-04}	7.3227×10^{-05}	0.644230
		14	1.1617×10^{-02}	4.9286×10^{-03}	3.8722×10^{-04}	0.708296

Table 4. The $Err_2, Err_\infty, Err_{rms}$ computed by Talbot's method for problem 2.

(α,β,γ)	m	m_T	Err_2	Err_∞	Err_{rms}	CPU (sec.)
$(1.3, 0.2, 0.9)$	22	30	2.2778×10^{-09}	8.4692×10^{-10}	1.0354×10^{-10}	1.387058
	25		5.2077×10^{-09}	2.4683×10^{-09}	2.0831×10^{-10}	2.893077
	28		5.9240×10^{-09}	1.8102×10^{-09}	2.1157×10^{-10}	4.540104
	30	20	6.8804×10^{-06}	4.3647×10^{-07}	2.2935×10^{-07}	4.290310
		25	1.5504×10^{-08}	1.7167×10^{-09}	5.1681×10^{-10}	5.406541
		30	9.2636×10^{-09}	2.3673×10^{-09}	3.0879×10^{-10}	6.253001
$(1.6, 0.5, 0.7)$	22	30	1.1655×10^{-09}	4.5895×10^{-10}	5.2979×10^{-11}	1.413894
	25		2.4327×10^{-09}	8.7358×10^{-10}	9.7309×10^{-11}	2.551745
	28		5.9798×10^{-09}	1.5282×10^{-09}	2.1357×10^{-10}	4.802169
	30	20	6.8807×10^{-06}	4.3647×10^{-07}	2.2936×10^{-07}	4.319773
		25	1.5690×10^{-08}	2.3208×10^{-09}	5.2301×10^{-10}	5.494691
		30	9.9438×10^{-09}	3.3832×10^{-09}	3.3146×10^{-10}	6.327990
$(1.9, 0.8, 0.5)$	22	30	9.5101×10^{-10}	3.0484×10^{-10}	4.3228×10^{-11}	1.500904
	25		1.6298×10^{-09}	5.9318×10^{-10}	6.5192×10^{-11}	2.605735
	28		3.3339×10^{-09}	1.4952×10^{-10}	1.1907×10^{-10}	4.379358
	30	20	6.8805×10^{-06}	4.3647×10^{-07}	2.2935×10^{-07}	4.246011
		25	1.5398×10^{-08}	1.2926×10^{-09}	5.1325×10^{-10}	5.247654
		30	6.2433×10^{-09}	3.0606×10^{-09}	2.0811×10^{-10}	6.329043

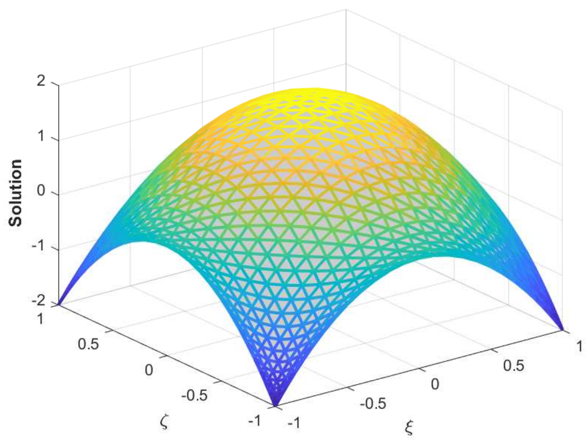

Figure 10. Numerical solution of problem 2 obtained by proposed scheme.

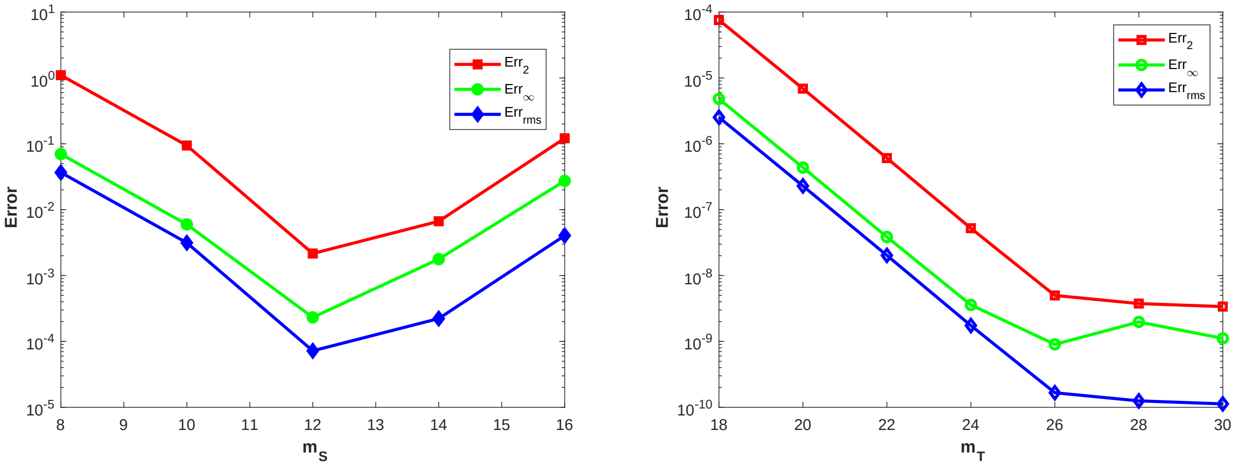

(a) **(b)**

Figure 11. (a) Plots of Err_2, Err_∞, and Err_{rms} obtained by Stehfest's method versus m_S and for $\alpha = 1.5, \beta = 0.7, \gamma = 0.3, t = 1$, and $m = 30$. (b) Plots of Err_2, Err_∞, and Err_{rms} obtained by Talbot's method versus m_T for $\alpha = 1.5, \beta = 0.7, \gamma = 0.3, t = 1$, and $m = 30$.

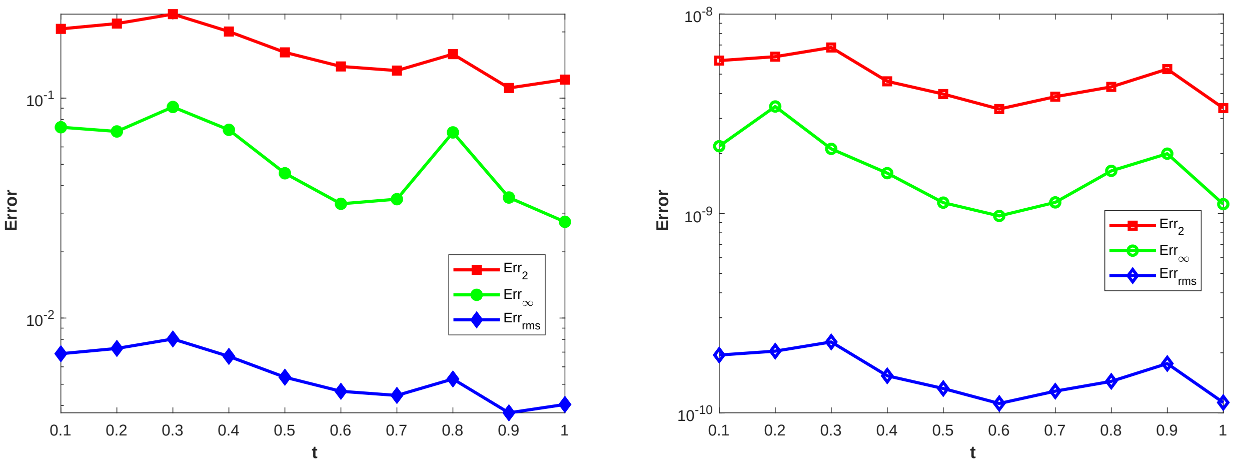

(a) **(b)**

Figure 12. (a) Plots of Err_2, Err_∞, and Err_{rms} obtained by Stehfest's method versus t for $\alpha = 1.5$, $\beta = 0.7$, $\gamma = 0.3$, $m_S = 14$, and $m = 30$. (b) Plots of Err_2, Err_∞, and Err_{rms} obtained by Talbot's method versus t for $\alpha = 1.5$, $\beta = 0.7$, $\gamma = 0.3$, $m_T = 30$, and $m = 30$.

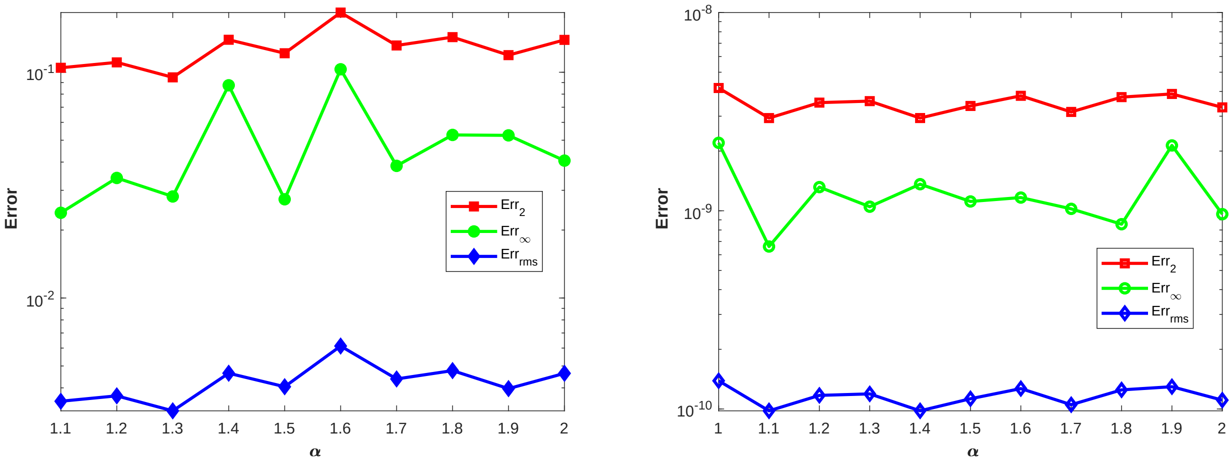

(a) **(b)**

Figure 13. (a) Plots of Err_2, Err_∞, and Err_{rms} obtained by Stehfest's method versus α for $\beta = 0.7,\ \gamma = 0.3,\ m_S = 14,\ t = 1$, and $m = 30$. (b) Plots of Err_2, Err_∞, and Err_{rms} obtained by Talbot's method versus α for $\beta = 0.7,\ \gamma = 0.3,\ m_T = 30,\ t = 1$, and $m = 30$.

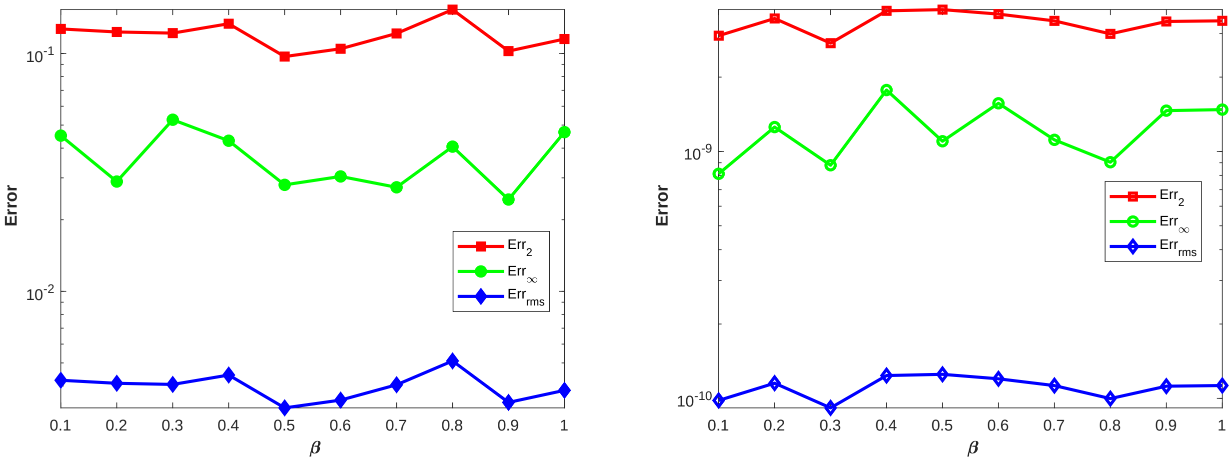

(a) **(b)**

Figure 14. (a) Plots of Err_2, Err_∞, and Err_{rms} obtained by Stehfest's method versus β for $\alpha = 1.5,\ \gamma = 0.3,\ m_S = 14,\ t = 1$, and $m = 30$. (b) Plots of Err_2, Err_∞, and Err_{rms} obtained by Talbot's method versus β for $\alpha = 1.5,\ \gamma = 0.3,\ m_T = 30,\ t = 1$, and $m = 30$.

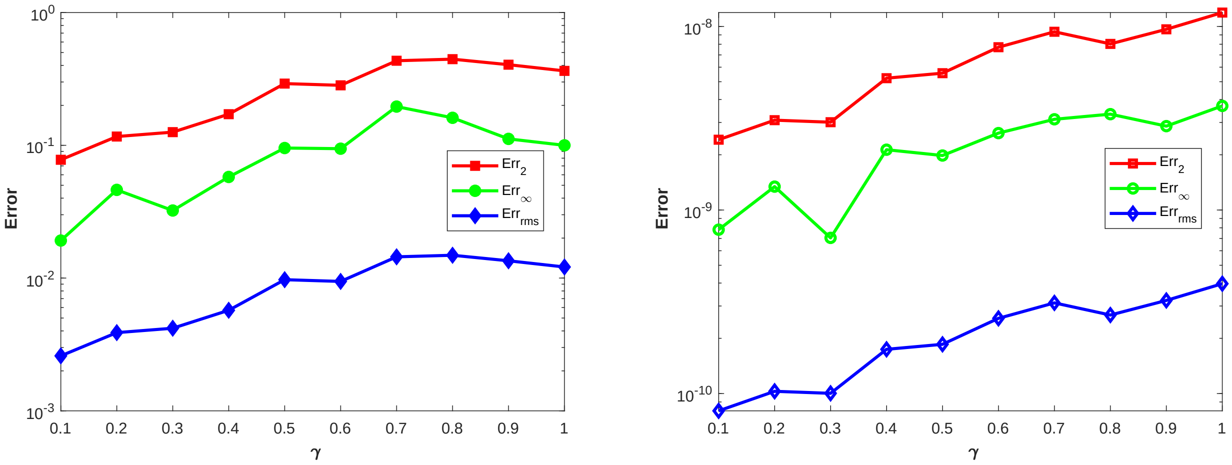

(a) **(b)**

Figure 15. (a) Plots of Err_2, Err_∞, and Err_{rms} versus γ obtained by Stehfest's method for $\alpha = 1.5,\ \beta = 0.7,\ m_S = 14,\ t = 1$, and $m = 30$. (b) Plots of Err_2, Err_∞, and Err_{rms} versus γ obtained by Talbot's method for $\alpha = 1.5,\ \beta = 0.7,\ m_T = 30,\ t = 1$, and $m = 30$.

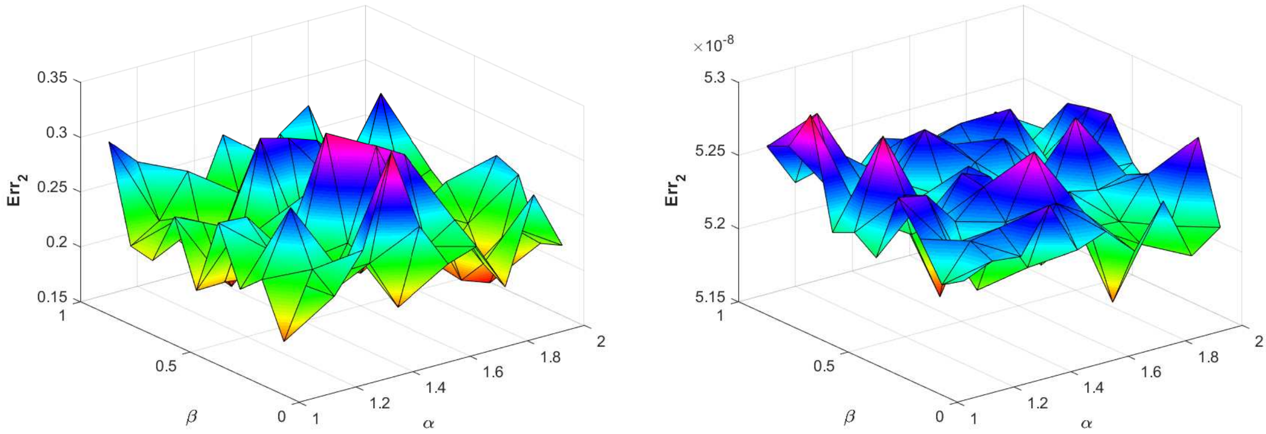

(a) **(b)**

Figure 16. (a) Plot of Err_2 versus α and β obtained by Stehfest's method for $\gamma = 0.5,\ t = 1,\ m_S = 16$, and $m = 30$. (b) Plot of Err_2 versus α and β obtained by Talbot's method for $\gamma = 0.5,\ t = 1,\ m_T = 24$, and $m = 30$.

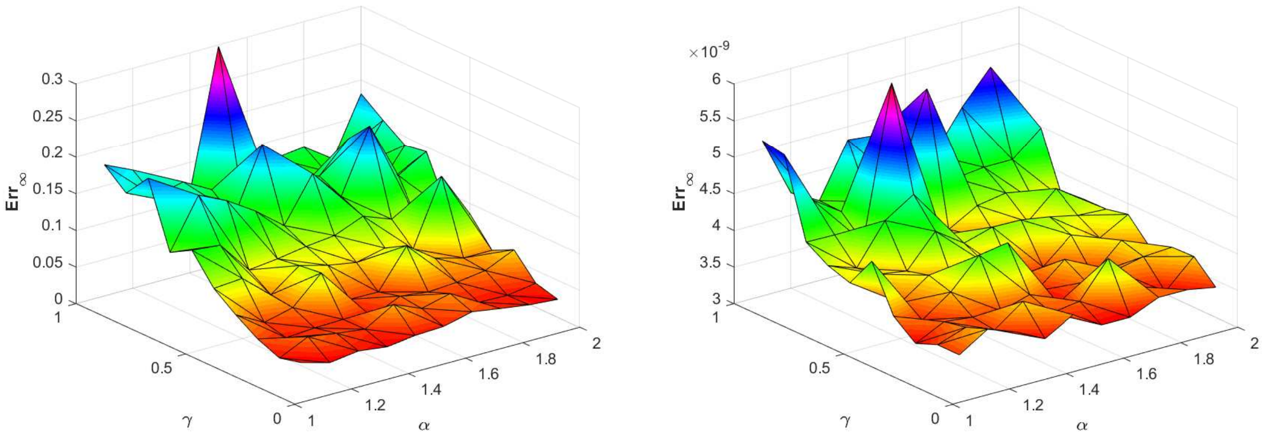

(a) **(b)**

Figure 17. (a) Plot of Err_∞ versus α and γ obtained by Stehfest's method for $\beta = 0.8,\ t = 1,\ m_S = 16$, and $m = 30$. (b) Plot of Err_∞ versus α and γ obtained by Talbot's method for $\beta = 0.8,\ t = 1,\ m_T = 24$, and $m = 30$.

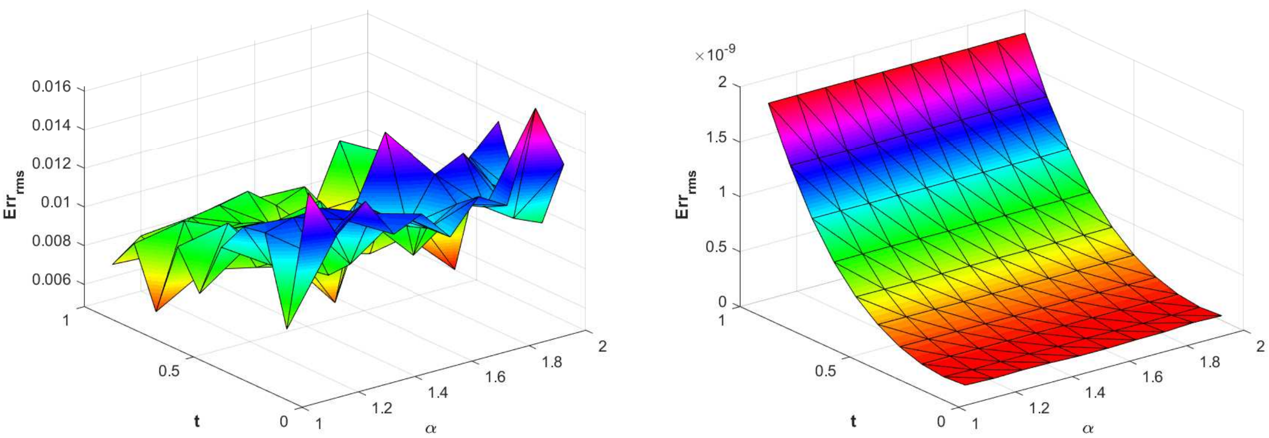

(a) **(b)**

Figure 18. (a) Plot of Err_{rms} versus α and t obtained by Stehfest's method for $\beta = 0.8,\ \gamma = 0.5,\ m_S = 16$, and $m = 30$. (b) Plot of Err_{rms} versus α and t obtained by Talbot's method for $\beta = 0.8,\ \gamma = 0.5,\ m_T = 24$, and $m = 30$.

Problem 3

We consider Eq (1.1) with analytical solution as

$$u(\xi,\zeta,t) = t^2 \sin(1-\xi)(e^{\xi}-1)\sin(1-\zeta)(e^{\zeta}-1)$$

and the source term is

$$\begin{aligned}\mathcal{G}(\xi,\zeta,t) = {} & \sin(1-\xi)(e^{\xi}-1)\sin(1-\zeta)(e^{\zeta}-1)\Big[\varrho_{1,1}\frac{2}{\Gamma(3-\alpha)}t^{2-\alpha} + 2\varrho_2 t + \varrho_{3,1}\frac{2}{\Gamma(3-\beta)}t^{2-\beta} + \varrho_4 t^2\Big] \\ & - \left(\varrho_5 t^2 + \varrho_6\frac{2}{\Gamma(3-\gamma)}t^{2-\gamma}\right)\Big[sin(\zeta-1)(e^{\zeta}-1)(2cos(\xi-1)e^{\xi} + sin(\xi-1)) \\ & + sin(\xi-1)(e^{\xi}-1)(2cos(\zeta-1)e^{\zeta} + sin(\zeta-1))\Big]\end{aligned}$$

where $\varrho_{1,1} = \varrho_2 = \varrho_{3,1} = \varrho_4 = \varrho_5 = \varrho_6 = 1$ and $\bar{\boldsymbol{\xi}} = (\xi,\zeta) \in [-1,1]^2$. The initial-boundary conditions are obtained from the analytical solution. The Err_2, Err_∞, and Err_{rms} errors obtained using the proposed method for problem 3 obtained via the Stehfest's and the Talbot's methods by using various values of m, m_T, m_S, α, β, γ, and $t = 1$ are presented in Tables 5 and 6, respectively.

The numerical method solution to problem 3 is shown in Figure 19. Figure 20 represents a comparison of error norms Err_2, Err_∞, and Err_{rms} computed by the Stehfest's and the Talbot's methods versus m_S and m_T with $\alpha = 1.5, \beta = 0.7$, $\gamma = 0.3$, $m = 30$, and $t = 1$. The comparison of Err_2, Err_∞, and Err_{rms} obtained using the Stehfest's and the Talbot's methods versus t with $\alpha = 1.5$, $\beta = 0.7$, $\gamma = 0.3$, $m_S = 14$, $m_T = 30$, and $m = 30$ is shown in Figure 21.

The comparison of Err_2, Err_∞, and Err_{rms} obtained using the Stehfest's and the Talbot's methods for different values of α with $\beta = 0.7$, $\gamma = 0.3$, $m = 30, m_S = 14$, $m_T = 30$, and $t = 1$ is shown in Figure 22. The comparison of Err_2, Err_∞, and Err_{rms} obtained using the Stehfest's and the Talbot's methods for different values of β with $\alpha = 1.5, \gamma = 0.7, m = 30, m_S = 14, m_T = 30$, and $t = 1$ is presented in Figure 23.

The comparison of Err_2, Err_∞, and Err_{rms} obtained using the Stehfest's and the Talbot's methods versus γ with $\alpha = 1.5, \beta = 0.7, m = 30, m_S = 14, m_T = 30$, and $t = 1$ is presented in Figure 24. The plot of Err_2 using the Stehfest's and the Talbot's methods for $\alpha \in [1,2]$ and $\beta \in [0,1]$ with $\gamma = 0.3$, $t = 1$, $m_S = 16, m_T = 30$, and $m = 30$ is shown in Figure 25.

In Figure 26, the plots of Err_∞ obtained using the Stehfest's and the Talbot's methods for $\alpha \in [1,2]$ and $\gamma \in [0,1]$ with $\beta = 0.7$, $t = 1$, $m_S = 16$, $m_T = 30$, and $m = 30$ are shown. Similarly, Figure 27 shows the plots of Err_{rms} using the Stehfest's and the Talbot's methods for $\alpha \in [1,2]$ and $t \in [0,1]$ with $\beta = 0.7, \gamma = 0.3, m_S = 16$, $m_T = 30$, and $m = 30$.

It is observed that the accuracy of the Stehfest's method steadily decreases for $m_S \geq 14$. From the results presented in tables and figures, we conclude that the proposed method is accurate, stable, and efficient. The numerical results demonstrates that the Talbot's method is more accurate than the Stehfest's method.

Table 5. The $Err_2, Err_\infty, Err_{rms}$ computed by Stehfest's method for problem 3.

(α,β,γ)	m	m_S	Err_2	Err_∞	Err_{rms}	CPU (sec.)
$(1.3, 0.2, 0.9)$	22	14	3.3480×10^{-05}	8.6337×10^{-06}	1.5218×10^{-06}	0.254196
	25		9.7449×10^{-05}	3.7684×10^{-05}	3.8980×10^{-06}	0.363822
	28		2.3165×10^{-04}	1.0850×10^{-04}	8.2733×10^{-06}	0.585754
	30	10	2.2116×10^{-04}	1.8488×10^{-05}	7.3719×10^{-06}	0.542104
		12	1.7804×10^{-04}	1.4958×10^{-05}	5.9348×10^{-06}	0.687321
		14	3.1175×10^{-04}	7.7178×10^{-05}	1.0392×10^{-06}	0.802970
$(1.6, 0.5, 0.7)$	22	14	3.0799×10^{-05}	1.0421×10^{-05}	1.4000×10^{-06}	0.191420
	25		8.6136×10^{-05}	3.5275×10^{-05}	3.4454×10^{-06}	0.339131
	28		1.4053×10^{-04}	4.7890×10^{-05}	5.0190×10^{-06}	0.559366
	30	10	2.2101×10^{-04}	1.8488×10^{-05}	7.3670×10^{-06}	0.583434
		12	1.8068×10^{-04}	1.4953×10^{-05}	6.0227×10^{-06}	0.673867
		14	1.2604×10^{-04}	4.4833×10^{-05}	4.2014×10^{-06}	0.733930
$(1.9, 0.8, 0.5)$	22	14	2.0609×10^{-05}	5.6164×10^{-06}	9.3675×10^{-07}	0.185813
	25		5.6168×10^{-05}	1.6845×10^{-05}	2.2467×10^{-06}	0.337030
	28		4.7054×10^{-05}	2.1159×10^{-05}	1.6805×10^{-06}	0.513103
	30	10	2.2103×10^{-04}	1.8488×10^{-05}	7.3676×10^{-06}	0.648050
		12	1.7979×10^{-04}	1.4953×10^{-05}	5.9930×10^{-06}	0.627418
		14	1.3026×10^{-04}	4.7709×10^{-05}	4.3420×10^{-06}	0.718273

Table 6. The $Err_2, Err_\infty, Err_{rms}$ computed by Talbot's method for problem 3.

(α,β,γ)	m	m_T	Err_2	Err_∞	Err_{rms}	CPU (sec.)
$(1.3, 0.2, 0.9)$	22	30	2.7733×10^{-11}	1.2506×10^{-11}	1.2606×10^{-12}	1.406847
	25		6.7413×10^{-11}	2.5993×10^{-11}	2.6965×10^{-12}	2.649332
	28		1.5151×10^{-11}	4.4017×10^{-11}	5.4112×10^{-12}	4.415065
	30	20	6.8451×10^{-08}	5.7242×10^{-09}	2.2817×10^{-09}	4.279803
		25	1.6659×10^{-10}	3.2206×10^{-11}	5.5531×10^{-12}	5.292333
		30	1.5071×10^{-10}	4.2789×10^{-11}	5.0236×10^{-12}	6.272503
$(1.6, 0.5, 0.7)$	22	30	2.4943×10^{-11}	1.2897×10^{-11}	1.1338×10^{-12}	1.503324
	25		5.4494×10^{-11}	1.8470×10^{-11}	2.1798×10^{-12}	2.687497
	28		1.1024×10^{-11}	3.6371×10^{-11}	3.9370×10^{-12}	4.498761
	30	20	6.8453×10^{-08}	5.7242×10^{-09}	2.2818×10^{-09}	4.177472
		25	1.4326×10^{-10}	3.6404×10^{-11}	4.7752×10^{-12}	5.148521
		30	1.3951×10^{-10}	6.3866×10^{-11}	4.6503×10^{-12}	6.443956
$(1.9, 0.8, 0.5)$	22	30	7.6747×10^{-12}	2.4080×10^{-12}	3.4885×10^{-13}	1.476408
	25		3.0024×10^{-11}	1.6923×10^{-11}	1.2010×10^{-12}	2.663378
	28		4.6899×10^{-11}	1.8591×10^{-11}	1.6750×10^{-12}	4.540820
	30	20	6.8448×10^{-08}	5.7242×10^{-09}	2.2816×10^{-09}	4.224953
		25	1.3981×10^{-10}	3.3329×10^{-11}	4.6602×10^{-12}	5.341039
		30	5.1002×10^{-11}	2.4527×10^{-11}	1.7001×10^{-12}	6.258475

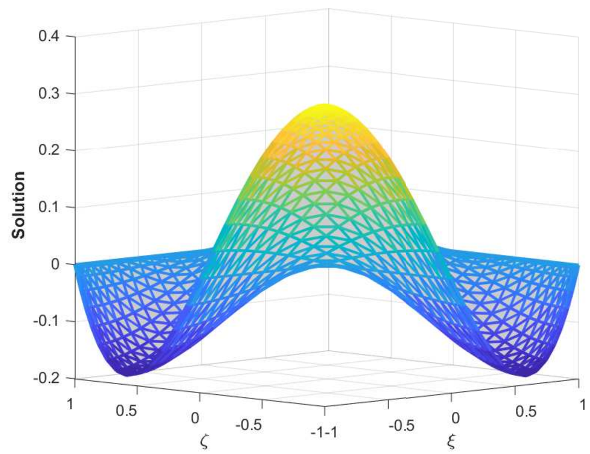

Figure 19. Numerical solution of problem 3 obtained by proposed scheme.

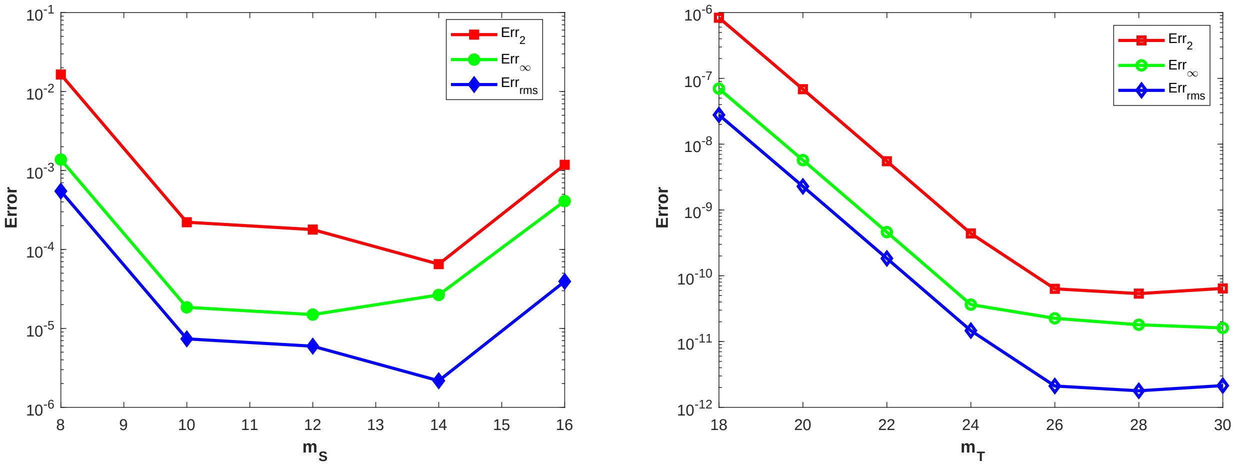

(a) **(b)**

Figure 20. (a) Plots of Err_2, Err_∞, and Err_{rms} obtained by Stehfest's method versus m_S and for $\alpha = 1.5, \beta = 0.7, \gamma = 0.3, t = 1$, and $m = 30$. (b) Plots of Err_2, Err_∞, and Err_{rms} obtained by Talbot's method versus m_T for $\alpha = 1.5, \beta = 0.7, \gamma = 0.3, t = 1$, and $m = 30$.

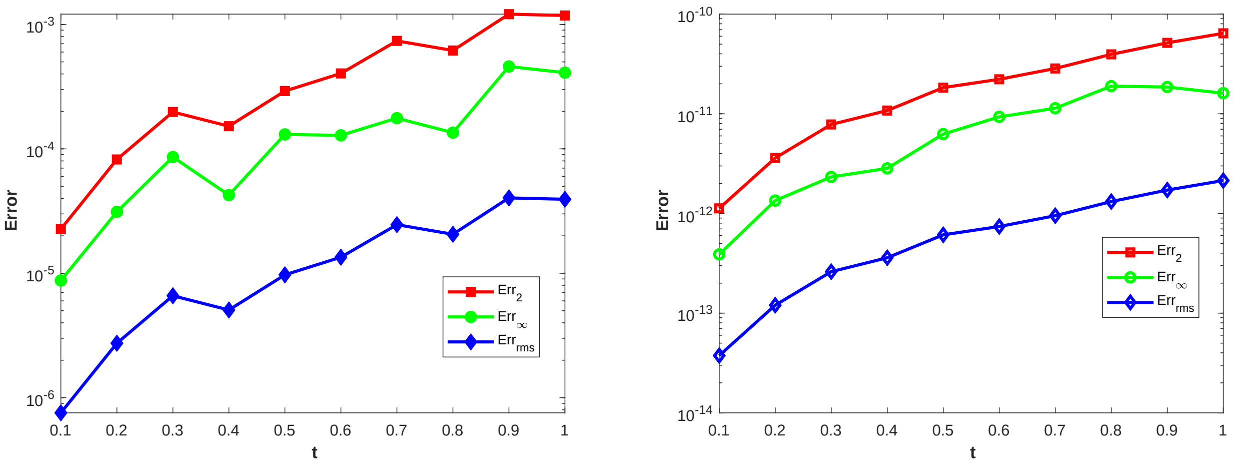

(a) **(b)**

Figure 21. (a) Plots of Err_2, Err_∞, and Err_{rms} obtained by Stehfest's method versus t for $\alpha = 1.5$, $\beta = 0.7$, $\gamma = 0.3$, $m_S = 14$, and $m = 30$. (b) Plots of Err_2, Err_∞, and Err_{rms} obtained by Talbot's method versus t for $\alpha = 1.5$, $\beta = 0.7$, $\gamma = 0.3$, $m_T = 30$, and $m = 30$.

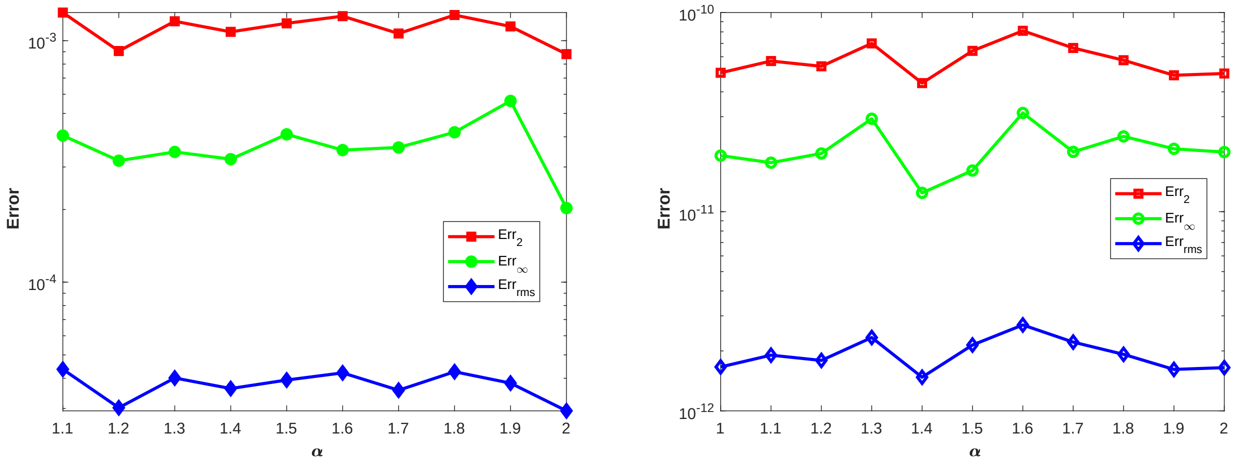

(a) **(b)**

Figure 22. (a) Plots of Err_2, Err_∞, and Err_{rms} obtained by Stehfest's method versus α for $\beta = 0.7,\ \gamma = 0.3,\ m_S = 14,\ t = 1$, and $m = 30$. (b) Plots of Err_2, Err_∞, and Err_{rms} obtained by Talbot's method versus α for $\beta = 0.7,\ \gamma = 0.3,\ m_T = 30,\ t = 1$, and $m = 30$.

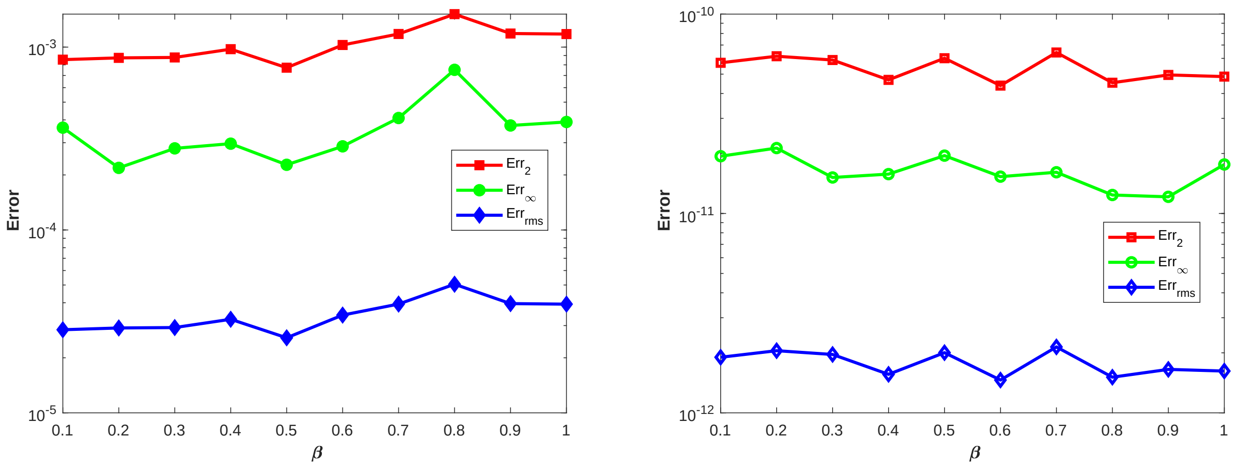

(a) **(b)**

Figure 23. (a) Plots of Err_2, Err_∞, and Err_{rms} obtained by Stehfest's method versus β for $\alpha = 1.5,\ \gamma = 0.3,\ m_S = 14,\ t = 1$, and $m = 30$. (b) Plots of Err_2, Err_∞, and Err_{rms} obtained by Talbot's method versus β for $\alpha = 1.5,\ \gamma = 0.3,\ m_T = 30,\ t = 1$, and $m = 30$.

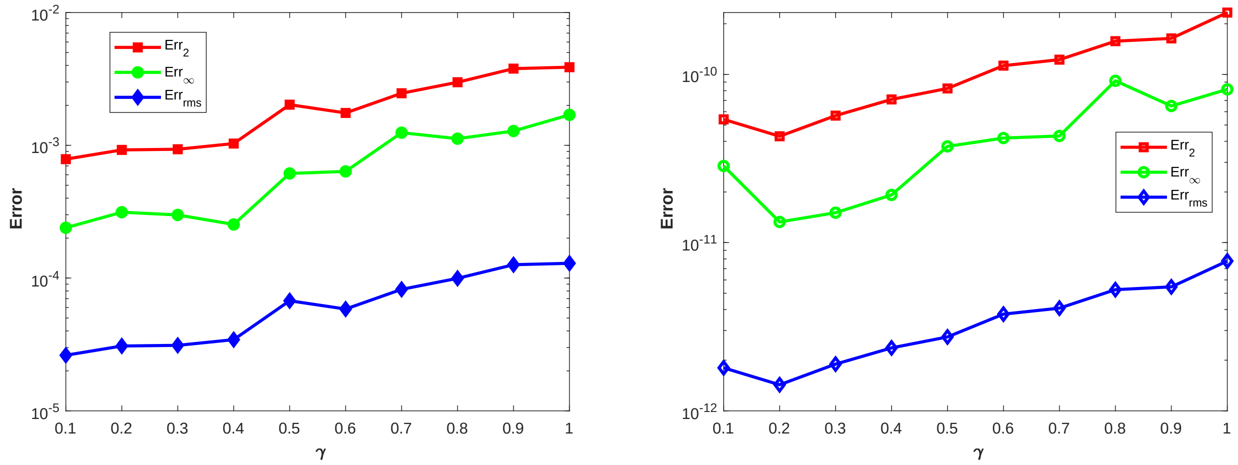

(a) **(b)**

Figure 24. (a) Plots of Err_2, Err_∞, and Err_{rms} versus γ obtained by Stehfest's method for $\alpha = 1.5,\ \beta = 0.7,\ m_S = 14,\ t = 1$, and $m = 30$. (b) Plots of Err_2, Err_∞, and Err_{rms} versus γ obtained by Talbot's method for $\alpha = 1.5,\ \beta = 0.7,\ m_T = 30,\ t = 1$, and $m = 30$.

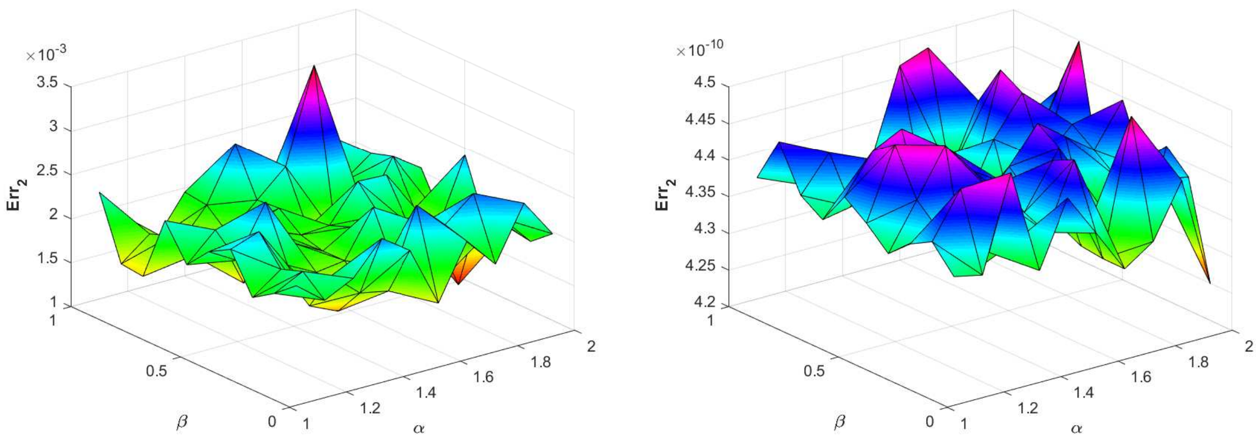

(a) **(b)**

Figure 25. (a) Plot of Err_2 versus α and β obtained by Stehfest's method for $\gamma = 0.5,\ t = 1,\ m_S = 16$, and $m = 30$. (b) Plot of Err_2 versus α and β obtained by Talbot's method for $\gamma = 0.5,\ t = 1,\ m_T = 24$, and $m = 30$.

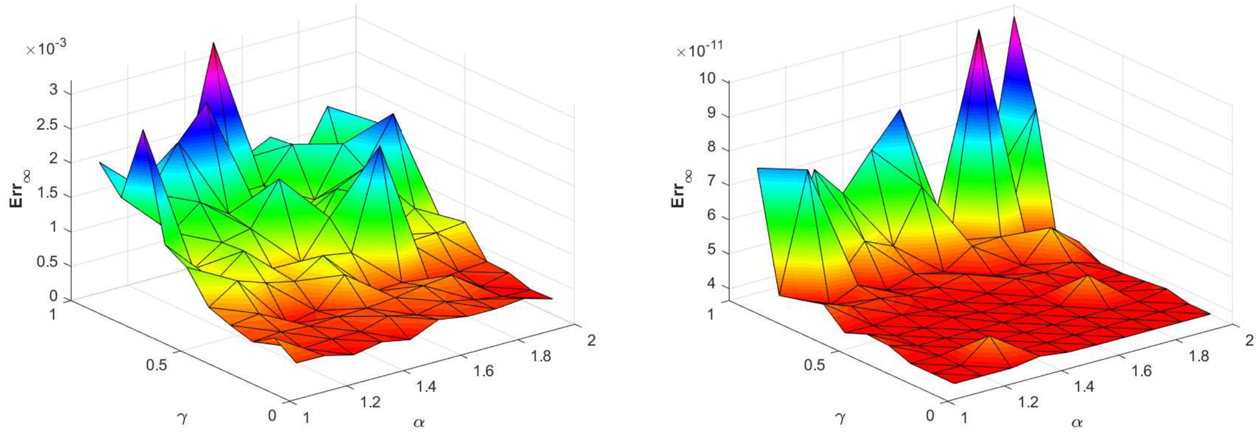

(a) **(b)**

Figure 26. (a) Plot of Err_∞ versus α and γ obtained by Stehfest's method for $\beta = 0.8,\ t = 1,\ m_S = 16$, and $m = 30$. (b) Plot of Err_∞ versus α and γ obtained by Talbot's method for $\beta = 0.8,\ t = 1,\ m_T = 24$, and $m = 30$.

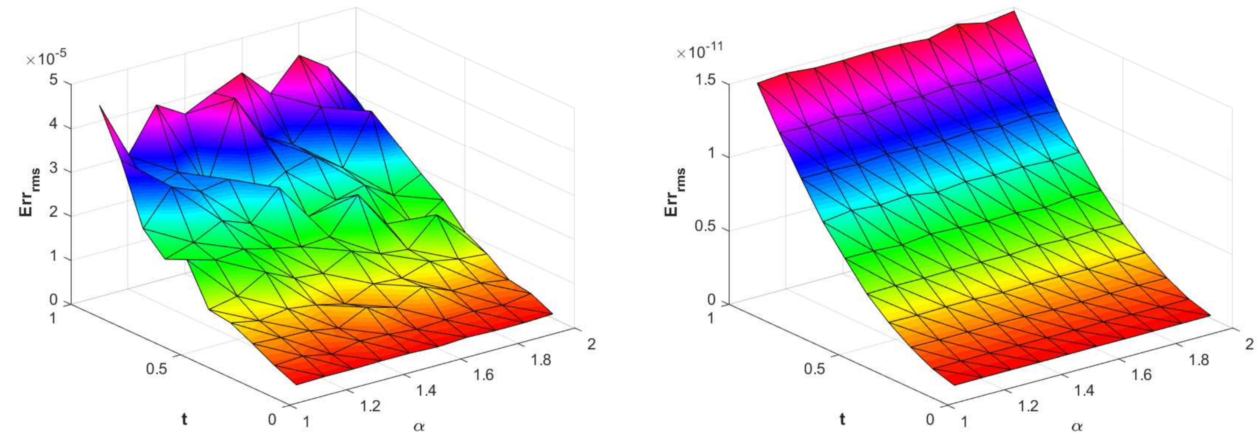

(a) **(b)**

Figure 27. (a) Plot of Err_{rms} versus α and t obtained by Stehfest's method for $\beta = 0.8,\ \gamma = 0.5,\ m_S = 16$, and $m = 30$. (b) Plot of Err_{rms} versus α and t obtained by Talbot's method for $\beta = 0.8,\ \gamma = 0.5,\ m_T = 24$, and $m = 30$.

Problem 4

We consider a limiting case of Eq (1.1) with analytical solution as

$$u(\xi, \zeta, t) = E_\gamma\Big(- \frac{\pi^2}{2} t^\gamma \Big) \cos\big(\frac{\pi}{2}\xi\big) \cos\big(\frac{\pi}{2}\zeta\big)$$

and the source term is

$$\mathcal{G}(\xi,\zeta,t) = E_{\gamma}\Big(-\frac{\pi^2}{2}t^{\gamma}\Big)\cos\big(\frac{\pi}{2}\xi\big)\cos\big(\frac{\pi}{2}\zeta\big)$$

where $\varrho_{1,1} = \varrho_{3,1} = \varrho_2 = 0$, $\varrho_6 = \varrho_4 = \varrho_5 = 1$, $(\xi,\zeta) \in [-1,1]^2$, and the initial-boundary conditions are obtained from the analytical solution. $E_{\gamma}(t) = \sum_{n=0}^{\infty} \frac{t^n}{\Gamma(n\gamma+1)}$, $(\gamma \in \mathbb{C}, Re(\gamma) > 0)$ is the Mittag Leffler function. The Err_2, Err_∞, and Err_{rms} errors of the proposed method for problem 4 by using various values of $m,\ m_T,\ m_S,\ \gamma$, and $t = 1$ are presented in Tables 7 and 8, respectively. The numerical solution of problem 4 is shown in Figure 28. Figure 29 presents a comparison of error norms Err_2, Err_∞, and Err_{rms} obtained via the Stehfest's and the Talbot's methods versus m_S and m_T with $\gamma = 0.7,\ m = 30$, and $t = 1$. The comparison of Err_2, Err_∞, and Err_{rms} obtained using the Stehfest's and the Talbot's methods versus t with $\gamma = 0.7,\ m_S = 14,\ m_T = 25$, and $m = 30$ is shown in Figure 30. The comparison of Err_2, Err_∞, and Err_{rms} using the Stehfest's and the Talbot's methods versus γ with $m = 30, m_S = 14, m_T = 25$, and $t = 1$ is presented in Figure 31. The plot of Err_2 using the Stehfest's and the Talbot's methods for $\gamma \in [0.5, 1]$ and $t \in [0, 1]$ with $m_S = 14, m_T = 25$, and $m = 30$ is shown in Figure 32. In Figure 33, the plots of Err_∞ computed using the Stehfest's and the Talbot's methods with $\gamma \in [0.5, 1],\ t \in [0, 1],\ m_S = 14,\ m_T = 25$, and $m = 30$ are shown. Similarly, Figure 34 shows the plot of Err_{rms} obtained using the Stehfest's and the Talbot's methods with $\gamma \in [0.5, 1],\ t \in [0, 1],\ m_S = 14,\ m_T = 25$, and $m = 30$. The computational results undeniably demonstrate that Talbot's method is greater in precision than Stehfest's method.

Table 7. The $Err_2, Err_\infty, Err_{rms}$ computed by Stehfest's method for problem 4.

	m	m_S	Err_2	Err_∞	Err_{rms}	CPU (sec.)
$\gamma = 0.5$	21	14	7.5454×10^{-05}	1.0208×10^{-05}	3.5930×10^{-06}	0.155965
	24		8.7095×10^{-05}	1.0340×10^{-05}	3.6290×10^{-06}	0.263790
	27		9.6493×10^{-05}	1.0212×10^{-05}	3.5738×10^{-06}	0.475612
	30	08	3.3892×10^{-05}	3.2475×10^{-06}	1.1297×10^{-06}	0.433870
		10	1.1589×10^{-04}	1.1104×10^{-05}	3.8630×10^{-06}	0.562005
		12	1.1026×10^{-04}	1.0576×10^{-05}	3.6754×10^{-06}	0.658822
$\gamma = 0.7$	21	14	8.2377×10^{-06}	1.7617×10^{-06}	3.9227×10^{-07}	0.156614
	24		7.5928×10^{-06}	1.5342×10^{-06}	3.1637×10^{-07}	0.263522
	27		1.4674×10^{-05}	3.3973×10^{-06}	5.4349×10^{-07}	0.459460
	30	08	2.2064×10^{-04}	2.1141×10^{-05}	7.3547×10^{-06}	0.428611
		10	2.3103×10^{-04}	2.2138×10^{-05}	7.7011×10^{-06}	0.567407
		12	3.1044×10^{-05}	2.9706×10^{-06}	1.0348×10^{-06}	0.623242
$\gamma = 0.9$	21	14	9.4376×10^{-05}	1.2762×10^{-05}	4.4941×10^{-06}	0.160795
	24		1.0828×10^{-04}	1.2942×10^{-05}	4.5116×10^{-06}	0.288674
	27		1.2360×10^{-04}	1.2863×10^{-05}	4.5779×10^{-06}	0.424751
	30	08	1.2649×10^{-03}	1.2120×10^{-04}	4.2162×10^{-05}	0.462303
		10	1.8471×10^{-03}	1.7699×10^{-04}	6.1570×10^{-05}	0.521154
		12	6.5184×10^{-04}	6.2457×10^{-05}	2.1728×10^{-05}	0.645028

Table 8. The $Err_2, Err_\infty, Err_{rms}$ computed by Talbot's method for problem 4.

	m	m_T	Err_2	Err_∞	Err_{rms}	CPU (sec.)
$\gamma = 0.5$	21	30	7.5633×10^{-05}	1.0211×10^{-05}	3.6016×10^{-06}	0.565917
	25		9.0040×10^{-05}	1.0253×10^{-05}	3.6016×10^{-06}	1.337206
	29		1.0445×10^{-04}	1.0278×10^{-05}	3.6016×10^{-06}	2.600535
	30	10	1.0893×10^{-04}	1.0438×10^{-05}	3.6311×10^{-06}	1.103470
		12	1.0800×10^{-04}	1.0348×10^{-05}	3.6000×10^{-06}	1.386152
		14	1.0804×10^{-04}	1.0353×10^{-05}	3.6015×10^{-06}	1.538342
$\gamma = 0.7$	21	30	3.2260×10^{-11}	4.3311×10^{-12}	1.5362×10^{-12}	0.598598
	25		3.8574×10^{-11}	4.3535×10^{-12}	1.5430×10^{-12}	1.348554
	29		4.3999×10^{-11}	4.2745×10^{-12}	1.5172×10^{-12}	2.666525
	30	12	7.2355×10^{-08}	6.9329×10^{-09}	2.4118×10^{-09}	1.266167
		16	2.8863×10^{-10}	2.7649×10^{-11}	9.6211×10^{-12}	1.678309
		20	4.5249×10^{-11}	4.3492×10^{-12}	1.5083×10^{-12}	2.078595
$\gamma = 0.9$	21	30	5.4576×10^{-12}	1.7432×10^{-12}	2.5989×10^{-13}	0.579733
	25		6.9966×10^{-12}	1.5988×10^{-12}	2.7987×10^{-13}	1.395903
	29		1.3880×10^{-11}	4.5894×10^{-12}	4.7862×10^{-13}	2.534978
	30	12	8.2775×10^{-08}	7.9314×10^{-09}	2.7592×10^{-09}	1.266089
		16	3.3689×10^{-10}	3.2289×10^{-11}	1.1230×10^{-11}	1.622688
		20	3.5520×10^{-12}	8.5037×10^{-13}	1.1840×10^{-13}	1.994124

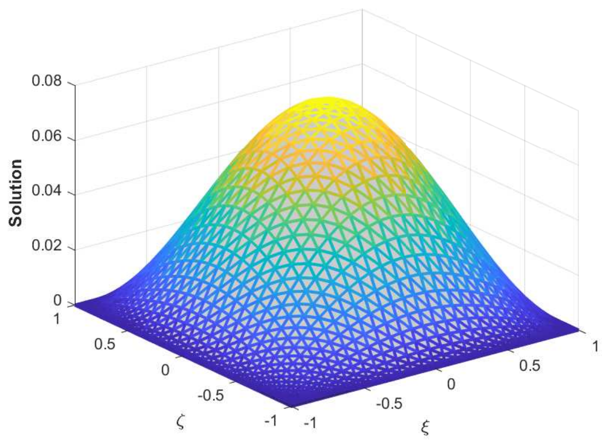

Figure 28. Numerical solution of problem 4 obtained by proposed scheme.

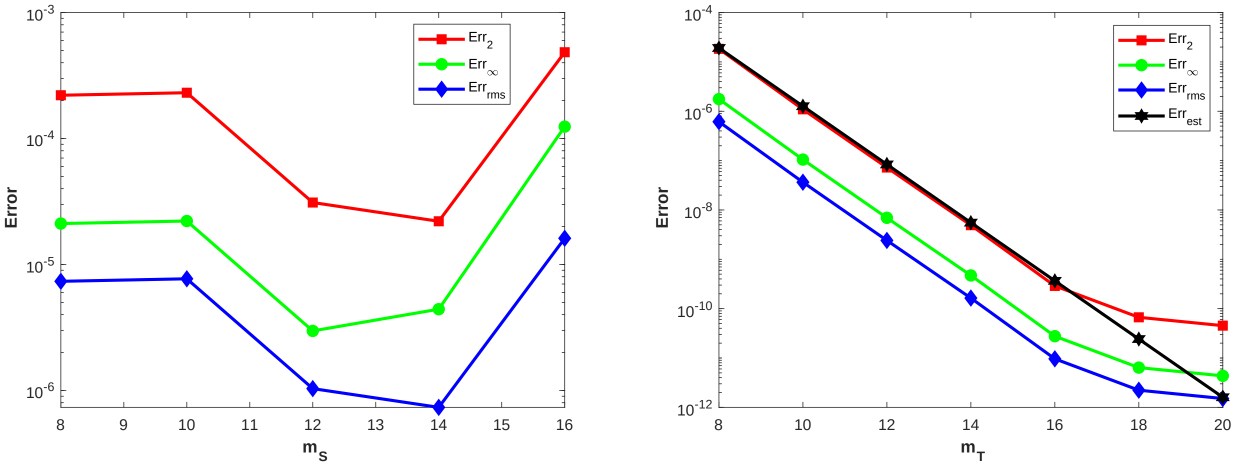

(a) (b)

Figure 29. (a) Plots of Err_2, Err_∞, and Err_{rms} obtained by Stehfest's method versus m_S and for $\gamma = 0.7, t = 1$, and $m = 30$. (b) Plots of Err_2, Err_∞, and Err_{rms} obtained by Talbot's method versus m_T for $\gamma = 0.7, t = 1$, and $m = 30$. It can be seen that the observed errors are in good agreement with theoretical error.

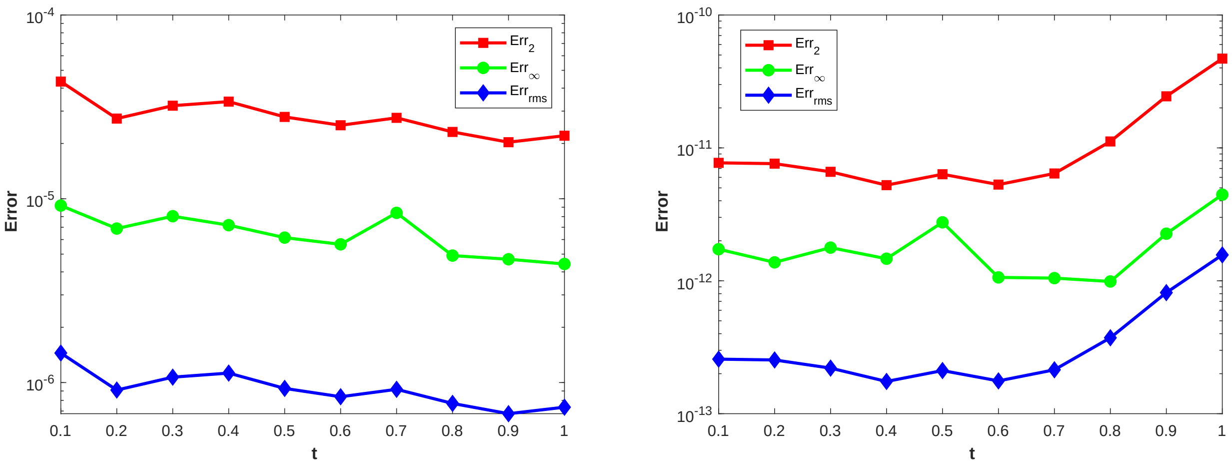

(a) (b)

Figure 30. (a) Plots of Err_2, Err_∞, and Err_{rms} obtained by Stehfest's method versus t for $\gamma = 0.7,\ m_S = 14$, and $m = 30$. (b) Plots of Err_2, Err_∞, and Err_{rms} obtained by Talbot's method versus t for $\gamma = 0.7,\ m_T = 25$, and $m = 30$.

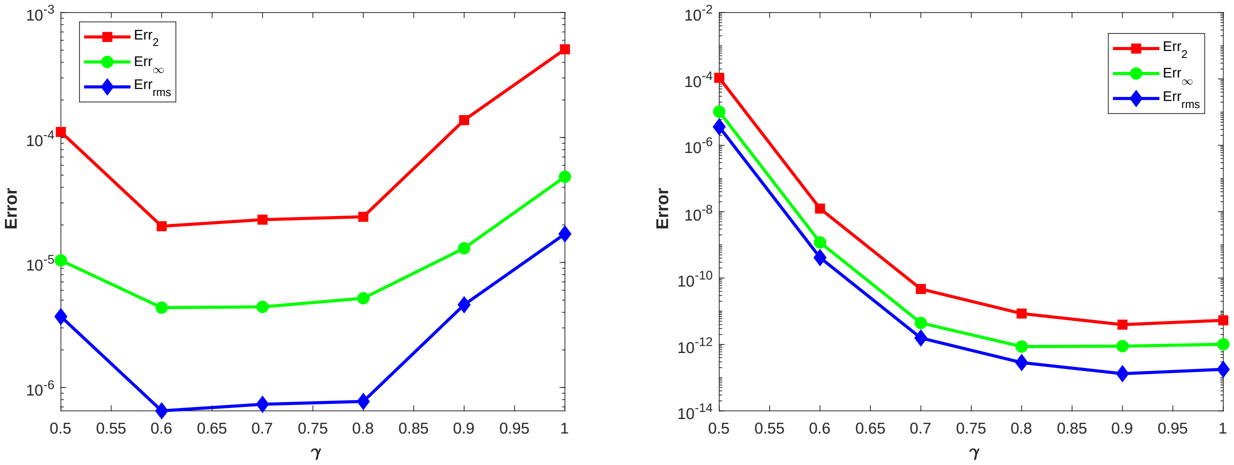

(a) **(b)**

Figure 31. (a) Plots of Err_2, Err_∞, and Err_{rms} versus γ obtained by Stehfest's method for $m_S = 14,\ t = 1$, and $m = 30$. (b) Plots of Err_2, Err_∞, and Err_{rms} versus γ obtained by Talbot's method for $m_T = 25,\ t = 1$, and $m = 30$.

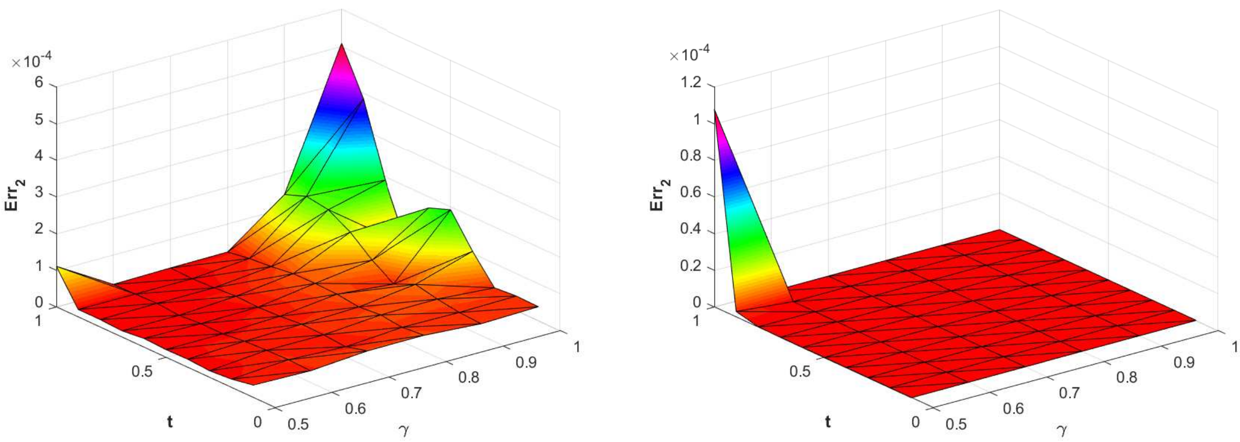

(a) **(b)**

Figure 32. (a) Plot of Err_2 versus γ and t obtained by Stehfest's method for $m_S = 14$, and $m = 30$. (b) Plot of Err_2 versus γ and t obtained by Talbot's method for $m_T = 25$, and $m = 30$.

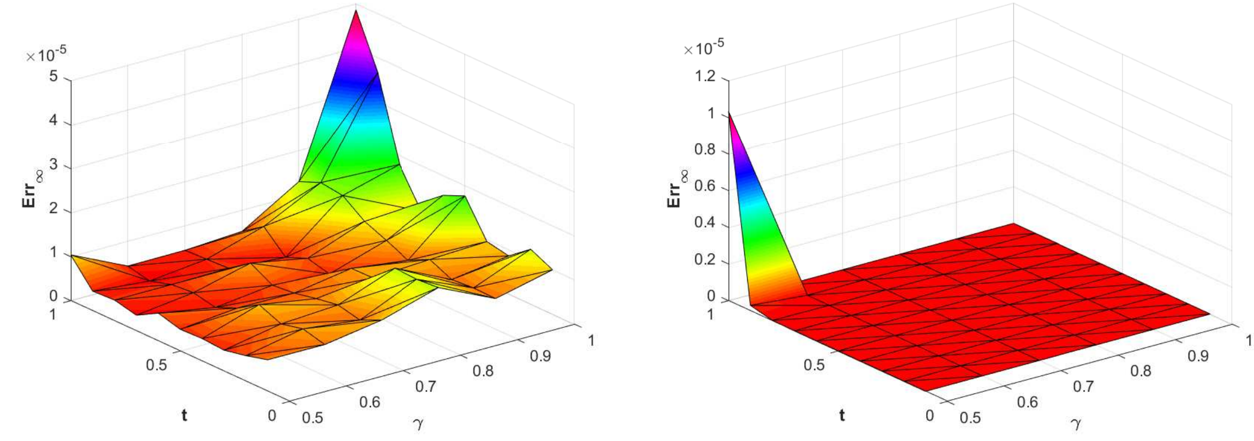

(a) **(b)**

Figure 33. (a) Plot of Err_∞ versus γ and t obtained by Stehfest's method for $m_S = 14$, and $m = 30$. (b) Plot of Err_∞ versus γ and t obtained by Talbot's method for $m_T = 25$, and $m = 30$.

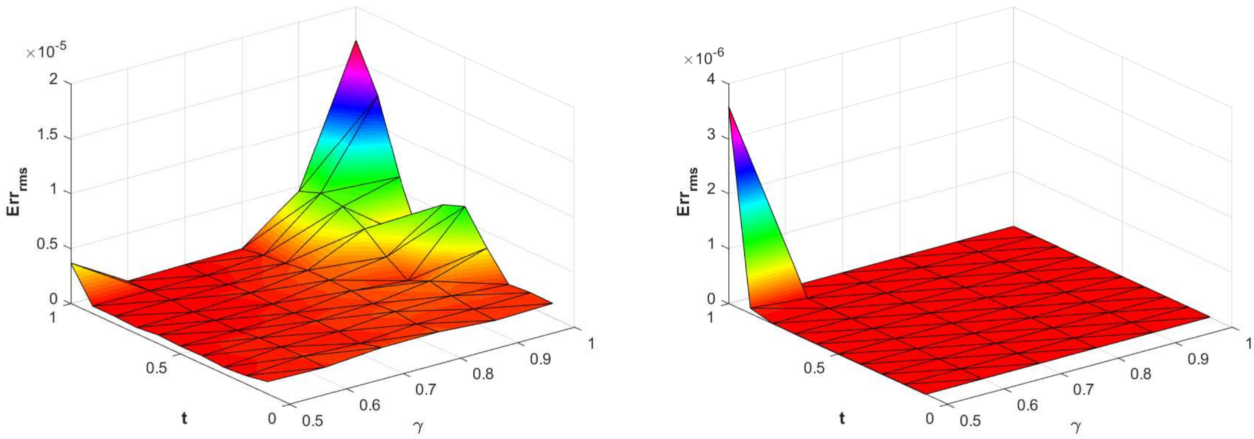

(a) **(b)**

Figure 34. (a) Plot of Err_{rms} versus γ and t obtained by Stehfest's method for $m_S = 14$, and $m = 30$. (b) Plot of Err_{rms} versus γ and t obtained by Talbot's method for $m_T = 25$, and $m = 30$.

3. Conclusion

In the current work, we have developed an efficient and stable numerical method, which combines the numerical Laplace transform method in time with the pseudospectral method in space for the numerical solution of the two-dimensional time fractional multi-term mixed sub-diffusion and diffusion-wave equation. The proposed method offers an excellent approach to the solution process of the considered equation. In our technique, first, the Laplace transform was employed, which reduced the problem into an elliptic problem in the Laplace transform domain, then the pseudospectral method was utilized to obtain the approximate solution to the transformed problem. Finally, the improved Talbot's method and the Stehfest's method were used to convert the obtained solution in Laplace transform domain back into time domain. The improved Talbot's method and the Stehfest's method provide a numerical inversion process that is accurate, stable, easy to implement, and does not suffer from stability issues which occur with finite difference time stepping methods. From the results presented in tables and figures, it can be observed that the Stehfest's method provides optimal results for $m_S < 14$, and for $m_S \geq 14$, its accuracy decreases. Furthermore, the obtained numerical results clearly demonstrate that the Talbot's method is considerably more precise than the Stehfest's method.

Use of AI tools declaration

The authors declare they have not used Artificial Intelligence (AI) tools in the creation of this article.

Acknowledgements

The authors D. Santina and N. Mlaiki would like to thank the Prince Sultan University for paying the publication fees for this work through TAS LAB. This research is supported by Prince Sultan University, Saudi Arabia.

Conflicts of interest

The authors declare that they have no conflicts of interest.

References

1. R. Metzler, J. Klafter, The random walk's guide to anomalous diffusion: A fractional dynamics approach, *Phys. Rep.*, **339** (2000), 1–77. https://doi.org/10.1016/S0370-1573(00)00070-3

2. Z. J. Fu, L. W. Yang, Q. Xi, C. S. Liu, A boundary collocation method for anomalous heat conduction analysis in functionally graded materials, *Comput. Math. Appl.*, **88** (2021), 91–109. https://doi.org/10.1016/j.camwa.2020.02.023

3. M. Bilal, T. Gul, A. Mouldi, S. Mukhtar, W. Alghamdi, S. M. Bouzgarrou, et al., Melting heat transition in a spinning flow of silver-magnesium oxide/engine oil hybrid nanofluid using parametric estimation, *J. Nanomater.*, **2022** (2022), 1–13. https://doi.org/10.1155/2022/2891315

4. Q. Xi, Z. Fu, T. Rabczuk, D. Yin, A localized collocation scheme with fundamental solutions for long-time anomalous heat conduction analysis in functionally graded materials, *Int. J. Heat Mass. Tran.*, **180** (2021), 121778. https://doi.org/10.1016/j.ijheatmasstransfer.2021.121778

5. Z. J. Fu, S. Reutskiy, H. G. Sun, J. Ma, M. A. Khan, A robust kernel-based solver for variable-order time fractional PDEs under 2D/3D irregular domains, *Appl. Math. Lett.*, **94** (2019), 105–111. https://doi.org/10.1016/j.aml.2019.02.025

6. J. A. T. Machado, A. M. Lopes, Analysis of natural and artificial phenomena using signal processing and fractional calculus, *Fract. Calc. Appl. Anal.*, **18** (2015), 459–478. https://doi.org/10.1515/fca-2015-0029
7. Hahim, S. Bouzgarrou, S. Rehman, E. Sabi, Thermodynamic analysis of Powell-Eyring-blood hybrid nanofluid through vertical stretching sheet with interface slip and melting heat, *Results Eng.*, **20** (2023), 101644. https://doi.org/10.1016/j.rineng.2023.101644
8. S. Bouzgarrou, M. Akermi, S. Nasr, F. Aouaini, A. H. Khan, K. Slimi, et al., CO_2 storage in porous media unsteady thermosolutal natural convection—Application in deep saline aquifer reservoirs, *Int. J. Greenh. Gas. Con.*, **125** (2023), 103890. https://doi.org/10.1016/j.ijggc.2023.103890
9. S. Bouzgarrou, H. S. Harzallah, K. Slimi, Unsteady double diffusive natural convection in porous media-application to CO_2 storage in deep saline aquifer reservoirs, *Energy Procedia*, **36** (2013), 756–765. https://doi.org/10.1016/j.egypro.2013.07.088
10. M. F. H. Lima, J. A. T. Machado, M. Crisóstomo, Experimental signal analysis of robot impacts in a fractional calculus perspective, *J. Adv. Comput. Intell.*, **11** (2007), 1079–1085. https://doi.org/10.20965/jaciii.2007.p1079
11. S. Qin, F. Liu, I. Turner, V. Vegh, Q. Yu, Q. Yang, Multi-term time-fractional Bloch equations and application in magnetic resonance imaging, *J. Comput. Appl. Math.*, **319** (2017), 308–319. https://doi.org/10.1016/j.cam.2017.01.018
12. C. Liu, N. Farouk, H. Ayed, F. Aouaini, S. M. Bouzgarrou, A. Mouldi, et al., Simulation of MHD free convection inside a square enclosure filled porous foam, *Case Stud. Therm. Eng.*, **32** (2022), 101901. https://doi.org/10.1016/j.csite.2022.101901
13. V. Srivastava, K. N. Rai, A multi-term fractional diffusion equation for oxygen delivery through a capillary to tissues, *Math. Comput. Model.*, **51** (2010), 616–624. https://doi.org/10.1016/j.mcm.2009.11.002
14. V. Daftardar-Gejji, S. Bhalekar, Boundary value problems for multi-term fractional differential equations, *J. Math. Anal. Appl.*, **345** (2008), 754–765. https://doi.org/10.1016/j.jmaa.2008.04.065
15. M. Stojanović, Numerical method for solving diffusion-wave phenomena, *J. Comput. Appl. Math.*, **235** (2011), 3121–3137. https://doi.org/10.1016/j.cam.2010.12.010
16. H. Jiang, F. Liu, I. Turner, K. Burrage, Analytical solutions for the multi-term time-space Caputo-Riesz fractional advection-diffusion equations on a finite domain, *J. Math. Anal. Appl.*, **389** (2012), 1117–1127. https://doi.org/10.1016/j.jmaa.2011.12.055
17. Y. Liu, L. Zheng, X. Zhang, Unsteady MHD Couette flow of a generalized Oldroyd-B fluid with fractional derivative, *Comput. Math. Appl.*, **61** (2011), 443–450. https://doi.org/10.1016/j.camwa.2010.11.021
18. J. Lin, S. Reutskiy, Y. Zhang, Y. Sun, J. Lu, The novel analytical-numerical method for multi-dimensional multi-term time-fractional equations with general boundary conditions, *Mathematics-Basel*, **11** (2023), 929. https://doi.org/10.3390/math11040929
19. F. Liu, S. Shen, V. Anh, I. Turner, Analysis of a discrete non-Markovian random walk approximation for the time fractional diffusion equation, *Anziam J.*, **46** (2004), C488–C504. https://doi.org/10.21914/anziamj.v46i0.973

20. Y. Zhao, F. Wang, X. Hu, Z. Shi, Y. Tang, Anisotropic linear triangle finite element approximation for multi-term time-fractional mixed diffusion and diffusion-wave equations with variable coefficient on 2D bounded domain, *Comput. Math. Appl.*, **78** (2019), 1705–1719. https://doi.org/10.1016/j.camwa.2018.11.028

21. Z. Liu, F. Liu, F. Zeng, An alternating direction implicit spectral method for solving two dimensional multi-term time fractional mixed diffusion and diffusion-wave equations, *Appl. Numer. Math.*, **136** (2019), 139–151. https://doi.org/10.1016/j.apnum.2018.10.005

22. J. Shen, X. M. Gu, Two finite difference methods based on an H_2N_2 interpolation for two-dimensional time fractional mixed diffusion and diffusion-wave equations, *Discrete Cont. Dyn-B.*, **27** (2022), 1179–1207. https://doi.org/10.3934/dcdsb.2021086

23. O. P. Agrawal, Solution for a fractional diffusion-wave equation defined in a bounded domain, *Nonlinear Dynam.*, **29** (2002), 145–155. https://doi.org/10.1023/A:1016539022492

24. C. Tadjeran, M. M. Meerschaert, H. P. Scheffler, A second-order accurate numerical approximation for the fractional diffusion equation, *J. Comput. Phys.*, **213** (2006), 205–213. https://doi.org/10.1016/j.jcp.2005.08.008

25. Y. Liu, H. Sun, X. Yin, L. Feng, Fully discrete spectral method for solving a novel multi-term time-fractional mixed diffusion and diffusion-wave equation, *Z. Angew. Math. Phys.*, **71** (2020), 1–19. https://doi.org/10.1007/s00033-019-1244-6

26. A. Bhardwaj, A. Kumar, A numerical solution of time-fractional mixed diffusion and diffusion-wave equation by an RBF-based meshless method, *Eng. Comput.-Germany*, **38** (2022), 1883–1903. https://doi.org/10.1007/s00366-020-01134-4

27. F. Safari, W. Chen, Coupling of the improved singular boundary method and dual reciprocity method for multi-term time-fractional mixed diffusion-wave equations, *Comput. Math. Appl.*, **78** (2019), 1594–1607. https://doi.org/10.1016/j.camwa.2019.02.001

28. H. Ye, F. Liu, I. Turner, V. Anh, K. Burrage, Series expansion solutions for the multi-term time and space fractional partial differential equations in two-and three-dimensions, *Eur. Phys. J.-Spec. Top.*, **222** (2013), 1901–1914. https://doi.org/10.1140/epjst/e2013-01972-2

29. Z. Li, O. Y. Imanuvilov, M. Yamamoto, Uniqueness in inverse boundary value problems for fractional diffusion equations, *Inverse Probl.*, **32** (2015), 015004. https://doi.org/10.1088/0266-5611/32/1/015004

30. S. S. Ezz-Eldien, E. H. Doha, Y. Wang, W. Cai, A numerical treatment of the two-dimensional multi-term time-fractional mixed sub-diffusion and diffusion-wave equation, *Commun. Nonlinear Sci.*, **91** (2020), 105445. https://doi.org/10.1016/j.cnsns.2020.105445

31. L. L. Sun, Y. S. Li, Y. Zhang, Simultaneous inversion of the potential term and the fractional orders in a multi-term time-fractional diffusion equation, *Inverse Probl.*, **37** (2021), 055007. https://doi.org/10.1088/1361-6420/abf162

32. B. Fornberg, *A Practical Guide to Pseudospectral Methods*, Cambridge: Cambridge University Press, 1998.

33. L. N. Trefethen, *Spectral Methods in MATLAB*, Philadelphia: Society for Industrial and Applied Mathematics, 2000. https://doi.org/10.1137/1.9780898719598

34. P. Maraner, E. Onofri, G. P. Tecchioli, Spectral methods in computational quantum mechanics, *J. Comput. Appl. Math.*, **37** (1991), 209–219. https://doi.org/10.1016/0377-0427(91)90119-5

35. C. Canuto, A. Quarteroni, M. Y. Hussaini, T. A. Zang, *Spectral Methods: Evolution to Complex Geometries and Applications to Fluid Dynamics*, Berlin: Springer, 2007. https://doi.org/10.1007/978-3-540-30728-0

36. W. Bourke, Spectral methods in global climate and weather prediction models. In: M. E. Schlesinger, *Physically-Based Modelling and Simulation of Climate and Climatic Change*, Dordrecht: Springer, **243** (1988), 169–220. https://doi.org/10.1007/978-94-009-3041-4_4

37. R. L. McCrory, S. A. Orszag, Spectral methods for multi-dimensional diffusion problems, *J. Comput. Phys.*, **37** (1980), 93–112. https://doi.org/10.1016/0021-9991(80)90006-6

38. K. Z. Korczak, A. T. Patera, An isoparametric spectral element method for solution of the Navier-Stokes equations in complex geometry, *J. Comput. Phys.*, **62** (1986), 361–382. https://doi.org/10.1016/0021-9991(86)90134-8

39. A. Bueno-Orovio, V. M. Perez-Garcia, F. H. Fenton, Spectral methods for partial differential equations in irregular domains: The spectral smoothed boundary method, *SIAM J. Sci. Comput.*, **28** (2006), 886–900. https://doi.org/10.1137/040607575

40. Z. J. Fu, W. Chen, H. T. Yang, Boundary particle method for Laplace transformed time fractional diffusion equations, *J. Comput. Phys.*, **235** (2013), 52–66. https://doi.org/10.1016/j.jcp.2012.10.018

41. Kamran, R. Kamal, G. Rahmat, K. Shah, On the numerical approximation of three-dimensional time fractional convection-diffusion equations, *Mathe. Probl. Eng.*, **2021** (2021), 4640476. https://doi.org/10.1155/2021/4640467

42. Kamran, M. Irfan, F. M. Alotaibi, S. Haque, N. Mlaiki, K. Shah, RBF-based local meshless method for fractional diffusion equations, *Fractal Fract.*, **7** (2023), 143. https://doi.org/10.3390/fractalfract7020143

43. L. Feng, F. Liu, I. Turner, Finite difference/finite element method for a novel 2D multi-term time-fractional mixed sub-diffusion and diffusion-wave equation on convex domains, *Commun. Nonlinear Sci.*, **70** (2019), 354–371. https://doi.org/10.1016/j.cnsns.2018.10.016

44. I. Podlubny, *Fractional Differential Equations: An introduction to fractional derivatives, fractional differential equations, to methods of their solution and some of their applications*, San Diego: Academic Press, 1999.

45. R. Razzaq, U. Farooq, J. Cui, T. Muhammad, Non-similar solution for magnetized flow of Maxwell nanofluid over an exponentially stretching surface, *Math. Probl. Eng.*, **2021** (2021), 5539542. https://doi.org/10.1155/2021/5539542

46. X. M. Gu, S. L. Wu, A parallel-in-time iterative algorithm for Volterra partial integro-differential problems with weakly singular kernel, *J. Comput. Phys.*, **417** (2020), 109576. https://doi.org/10.1016/j.jcp.2020.109576

47. B. D. Welfert, Generation of pseudospectral differentiation matrices I, *SIAM J. Numer. Anal.*, **34** (1997), 1640–1657. https://doi.org/10.1137/S0036142993295545
48. A. Shokri, S. Mirzaei, A pseudo-spectral based method for time-fractional advection-diffusion equation, *Comput. Methods Diffe.*, **8** (2020), 454–467. https://doi.org/10.22034/CMDE.2020.29307.1414
49. R. Baltensperger, M. R. Trummer, Spectral differencing with a twist, *SIAM J. Sci. Comput.*, **24** (2003), 1465–1487. https://doi.org/10.1137/S1064827501388182
50. S. Börm, L. Grasedyck, W. Hackbusch, Introduction to hierarchical matrices with applications, *Eng. Anal. Bound. Elem.*, **27** (2003), 405–422. https://doi.org/10.1016/S0955-7997(02)00152-2
51. B. Dingfelder, J. A. C. Weideman, An improved Talbot method for numerical Laplace transform inversion, *Numer. Algorithms*, **68** (2015), 167–183. https://doi.org/10.1007/s11075-014-9895-z
52. H. Stehfest, Algorithm 368: Numerical inversion of Laplace transforms [D5], *Commun. ACM*, **13** (1970), 47–49. Available from: https://dl.acm.org/doi/pdf/10.1145/361953.361969.
53. A. Talbot, The accurate numerical inversion of Laplace transforms, *IMA J. Appl. Math.*, **23** (1979), 97–120. https://doi.org/10.1093/imamat/23.1.97
54. Kamran, U. Gul, F. M. Alotaibi, K. Shah, T. Abdeljawad, Computational approach for differential equations with local and nonlocal fractional-order differential operators, *J. Math.-UK*, **2023** (2023), 6542787. https://doi.org/10.1155/2023/6542787
55. Kamran, S. Ahmad, K. Shah, T. Abdeljawad, B. Abdalla, On the approximation of fractal-fractional differential equations using numerical inverse laplace transform methods, *CMES-Comp. Model. Eng.*, **135** (2023), 2743–2765. https://doi.org/10.32604/cmes.2023.023705
56. D. P. Gaver Jr, Observing stochastic processes, and approximate transform inversion, *Oper. Res.*, **14** (1966), 444–459. https://doi.org/10.1287/opre.14.3.444
57. A. Kuznetsov, On the convergence of the Gaver–Stehfest algorithm, *SIAM J. Numer. Anal.*, **51** (2013), 2984–2998. https://doi.org/10.1137/13091974X
58. B. Davies, B. Martin, Numerical inversion of the Laplace transform: A survey and comparison of methods, *J. Comput. Phys.*, **33** (1979), 1–32. https://doi.org/10.1016/0021-9991(79)90025-1
59. J. Abate, W. Whitt, A unified framework for numerically inverting Laplace transforms, *Informs J. Comput.*, **18** (2006), 408–421. https://doi.org/10.1287/ijoc.1050.0137